

On the efficiency of Stochastic Quasi-Newton Methods for Deep Learning

Mahsa Yousefi^a, Ángeles Martínez^{a,*}

^a*Department of Mathematics and Geosciences, University of Trieste, via Valerio 12/1, 34127 Trieste, Italy*

Abstract

While first-order methods are popular for solving optimization problems that arise in large-scale deep learning problems, they come with some acute deficiencies. To diminish such shortcomings, there has been recent interest in applying second-order methods such as quasi-Newton based methods which construct Hessians approximations using only gradient information. The main focus of our work is to study the behaviour of stochastic quasi-Newton algorithms for training deep neural networks. We have analyzed the performance of two well-known quasi-Newton updates, the limited memory Broyden-Fletcher-Goldfarb-Shanno (BFGS) and the Symmetric Rank One (SR1). This study fills a gap concerning the real performance of both updates and analyzes whether more efficient training is obtained when using the more robust BFGS update or the cheaper SR1 formula which allows for indefinite Hessian approximations and thus can potentially help to better navigate the pathological saddle points present in the non-convex loss functions found in deep learning. We present and discuss the results of an extensive experimental study which includes the effect of batch normalization and network's architecture, the limited memory parameter, the batch size and the type of sampling strategy. we show that stochastic quasi-Newton optimizers are efficient and able to outperform in some instances the well-known first-order Adam optimizer run with the optimal combination of its numerous hyperparameters.

Keywords: nonlinear programming, stochastic quasi-Newton methods, BFGS, SR1, deep neural networks

2010 MSC: 90C30, 90C06, 90C53, 90C90, 65K05

1. Introduction

Deep learning (DL) as a leading technique of machine learning (ML) has attracted much attention and become one the most popular directions of research. DL approaches have been applied to solve many large-scale problems in different fields, e.g., automatic machine translation, image recognition, natural language processing, fraud detection, etc, by training deep neural networks (DNNs) over large available datasets. Deep Learning problems are often posed as unconstrained optimization problems. In supervised learning, the goal is to minimize the empirical risk of the model (DNN) by finding an optimal parametric mapping function

*Corresponding author

Email addresses: mahsa.yousefi@phd.units.it (Mahsa Yousefi), amartinez@units.it (Ángeles Martínez)

$$h(\cdot; w) : \mathbb{R}^n \longrightarrow \mathbb{R}$$

$$\min_{w \in \mathbb{R}^n} F(w) \triangleq \frac{1}{N} \sum_{i=1}^N L(y_i, h(x_i; w)) \triangleq \frac{1}{N} \sum_{i=1}^N L_i(w), \quad (1)$$

where $w \in \mathbb{R}^n$ is the vector of trainable parameters of the model and (x_i, y_i) denotes the i th sample pair in the available training dataset $\{(x_i, y_i)\}_{i=1}^N$ with input x_i and target y_i . Moreover, $L_i(w)$ is a loss function defining the prediction error between the model computed value $h(x_i; w)$ and the target y_i . For solving the large-scale problem (1) which is highly nonlinear and often non-convex, applying traditional optimization algorithms developed for scientific computing and other related areas is ineffective. That is why much effort has recently been devoted to the development of DL optimization algorithms. From the point of view of gradient information, popular optimization methods can be divided into two general categories: *first-order methods* such as gradient descent with update equation $w_{k+1} = w_k - \eta \nabla F(w_k)$ and *second-order methods* such as Newton method with update $w_{k+1} = w_k - \eta \nabla^2 F(w_k)^{-1} \nabla F(w_k)$, where $\nabla F(w_k)$ and $\nabla^2 F(w_k)$ are the true gradient vector and Hessian matrix at point w_k , and η and w_k denote the learning rate and network parameters at iteration k , respectively. These methods, in turn, fall into two broad categories, stochastic and deterministic, in which either one sample (or a small subset of samples called mini-batch) or a single batch composed of all samples are, respectively, employed in the evaluation of the function or gradient and other required computations. In DL applications both N and n can be very large thus computing the full gradient is expensive and computations involving the true Hessian or its approximations may not be practical. Stochastic optimization methods to overcome the aforementioned issues has become the usual approach.

1.1. Literature review

Stochastic first-order methods have been widely used in many DL applications due to their low per-iteration cost, optimal complexity, easy implementation and proven efficiency in practice. The preferred method is the stochastic gradient descent (SGD) method [40, 9], and its variance-reduced [15, 25, 41] and adaptive [16, 26] variants. However, due to the use of first-order information only, these methods come with several issues such as relatively-slow convergence, highly sensitivity to the choice of hyper-parameters (e.g., step-length and batch size), stagnation at high training loss, difficulty in escaping saddle points [48], limited benefits of parallelism due to usual implementation with small mini-batches and suffering from ill-conditioning [28].

On the other hand, second order methods can often find good minima in fewer steps due to their use of curvature information. The main second order method incorporating the inverse Hessian matrix is Newton's method [38], but it presents serious computational and memory usage challenges involved in the computation of the Hessian, in particular for large-scale DL problems; see [8] for details.

Quasi-Newton [38] and Hessian-free Newton methods [33] are two techniques aimed at incorporating second order information without computing and storing the true Hessian matrix. Hessian-free methods attempt to find an approximate Newton direction using conjugate gradient methods [32, 6, 47]. The major challenge of these methods is the linear system with an indefinite sub-sample Hessian matrix and (sub-sampled) gradient vector to be solved at each Newton step. This problem can be solved in the trust-region framework by the

CG-Steihaug algorithm [43]. Nevertheless, whether true Hessian matrix-vector products or subsampled variants of them, see e.g. [47], are used, the iteration complexity of a (modified) CG algorithm is significantly greater than that of a limited memory quasi-Newton method, i.e. stochastic L-BFGS; see complexity table in [47]. In fact, quasi-Newton methods and their limited memory variants [38] attempt to combine the speed of Newton’s method and the scalability of first-order methods. They construct Hessian approximations using only gradient information and exhibit superlinear convergence. All these methods can be implemented to take benefit from parallelization in the evaluations of the objective function and its derivatives, which is possible due to their finite sum structure [8, 24, 2].

Quasi-Newton and stochastic quasi-Newton methods to solve large optimization problems arising in machine learning have been recently extensively considered within the context of convex and non-convex optimization. Stochastic quasi-Newton methods use a subsampled Hessian approximation or/and subsampled gradient. In [42], a stochastic Broyden-Fletcher-Goldfarb-Shanno (BFGS) and its limited memory variant (L-BFGS) were proposed for online convex optimization in [42]. Another stochastic L-BFGS method for solving strongly convex problems was presented in [12] that uses sampled Hessian-vector products rather than gradient differences, which was proved in [37] to be linearly convergent by incorporating the variance reduction technique (SVRG [25]) to alleviate the effect of noisy gradients. A closely related variance reduced block L-BFGS method was proposed in [21]. A regularized stochastic BFGS method was proposed in [34], and an online L-BFGS method was proposed in [35] for strongly convex problems and extended in [31] to incorporate SVRG variance reduction. For the solution of non-convex optimization problems arising in deep learning, a damped L-BFGS method incorporating SVRG variance reduction was developed and its convergence properties were studied in [44]. Some of these stochastic quasi-Newton algorithms employ fixed size batches and compute stochastic gradient differences in a stable way, originally proposed in [42], using the same batch at the beginning and at the end of the iteration. Since this can potentially double the iteration complexity, an overlap batching strategy was proposed to reduce the computational cost in [3] and tested also in [4]. This strategy was further applied in [17, 39]. Other stochastic quasi-Newton methods have been considered that employ a progressive batching approach in which the sample size is increased as the iteration progresses, see e.g. [7, 5] and references therein. Recently, in [19] a Kronecker-factored block diagonal BFGS and L-BFGS method was proposed, that takes advantage of the structure of feed-forward DNN training problems.

1.2. Contribution and outline

The BFGS update is the most widely-used type of quasi-Newton method for general optimization and the most widely considered quasi-Newton method for general machine learning and deep learning. Almost all the previously cited articles considered BFGS, with only few exceptions using the Symmetric Rank One (SR1) update instead [17]. However, a clear disadvantage of BFGS occurs if one tries to enforce positive definiteness of the approximated Hessian matrices in a non-convex setting. In this case, BFGS has the difficult task of approximating an indefinite matrix (the true Hessian) with a positive-definite matrix which can result in the generation of nearly-singular Hessian approximations.

In this paper, we analyze the behaviour of both updates on real modern deep neural network architectures and try to determine whether more efficient training can be obtained when using the BFGS update or the cheaper SR1 formula that allows for indefinite Hessian

approximations and thus can potentially help to better navigate the pathological saddle points present in the non-convex loss functions found in deep learning. We study the performance of both quasi-Newton methods in the trust-region (TR) framework for solving (1) onto realistic large-size DNNs. We introduce stochastic variants of the two quasi-Newton updates based on an overlapping sampling strategy which is well-defined within the TR approach. We have implemented and applied these algorithms to train convolutional and residual neural networks ranging from a shallow LeNet-like network to a self-built network with and without batch normalization layers and the modern ResNet-20 for image classification problems. We have compared the performance of both stochastic quasi-Newton methods with another stochastic quasi-Newton algorithm based on a progressive batching strategy and with the first-order Adam optimizer running with the optimal values of its hyper-parameters obtained by grid searching.

The paper is organized as follows: [Section 2](#) provides a general overview on (stochastic) quasi-Newton methods within the TR approach for solving problem (1). In [Section 3](#) and [Section 4](#), respectively, two training algorithms named L-BFGS-TR and L-SR1-TR are described. In [Section 5](#), we describe the sampling strategy and the stochastic variants of both methods. Our empirical study and a summary of the results are presented in [Section 6](#). Finally, some concluding remarks are given in [Section 7](#).

2. Quasi-Newton based optimization

Quasi-Newton (QN) methods (see, e.g. [38]), as important developments in the field of nonlinear optimization are applicable for both convex and non-convex problems. Let

$$\begin{aligned} f_k &\triangleq F(w_k) = \frac{1}{N} \sum_{i=1}^N L_i(w_k), \\ g_k &\triangleq \nabla F(w_k) = \frac{1}{N} \sum_{i=1}^N \nabla L_i(w_k), \\ B_k &\approx \nabla^2 F(w_k) = \frac{1}{N} \sum_{i=1}^N \nabla^2 L_i(w_k). \end{aligned} \tag{2}$$

A QN method is given by

$$w_{k+1} = w_k + \eta B_k g_k, \tag{3}$$

where the symmetric low-rank QN matrices B_k are approximations to the Hessian matrix constructed using gradient information and satisfy the following *secant equation*

$$B_{k+1} s_k = y_k, \tag{4}$$

where

$$s_k = p_k, \quad y_k = g_t - g_k, \tag{5}$$

in which $g_t \triangleq \nabla F(w_t)$ and the vector p_k is a search direction obtained using line search or TR approaches in order to propose a trial parameters vector as

$$w_t = w_k + p_k. \tag{6}$$

For solving the DL optimization problem (1), TR methods [14] generate a sequence of iterates as (6) such that the search direction p_k is obtain by solving the following TR subproblem

$$p_k = \arg \min_{p \in \mathbb{R}^n} Q_k(p) \triangleq \frac{1}{2} p^T B_k p + g_k^T p \quad \text{s.t.} \quad \|p\|_2 \leq \delta_k, \quad (7)$$

for some TR radius $\delta_k > 0$. Accepting the update (6) is subject to the value of the ratio between the actual reduction in the objective function of (1) and the reduction predicted by the quadratic model of (7), that is

$$\rho_k = \frac{f_k - f_t}{Q_k(0) - Q_k(p_k)}, \quad (8)$$

where $f_t \triangleq F(w_t)$. Therefore, since the denominator in (8) is nonnegative, if ρ_k is positive then $w_{k+1} \triangleq w_t$; otherwise, $w_{k+1} \triangleq w_k$.

Using a TR method over line search for computing p_k presents some advantages. According to [11, 10], the subproblem (7) can be efficiently solved if the Hessian approximation B_k is chosen to be a QN matrix. Another primary advantage of using a TR method is that it can accommodate both positive definite and indefinite Hessian approximations more easily. Moreover, the progress of the learning process will not stop or slow down even in presence of occasional step rejection; i.e. when $w_{k+1} \triangleq w_k$.

For solving (7), the computational bottleneck of most TR methods, there are generally the following approaches:

Iterative approach. In large-scale optimization problems, Dogleg method with positive definite B_k and 2D subspace minimization method with indefinite B_k can be used [38].

Direct approach. Using the Euclidean norm (2-norm) to define the subproblem (7) leads to characterize the global solution of (7) by the optimality conditions given in the following theorem from Gay [18] and Moré and Sorensen [36]:

Theorem 2.1. *Let δ be a given positive constant. A vector p^* is a global solution of the trust-region problem (7) if and only if $\|p^*\|_2 \leq \delta$ and there exists a unique $\sigma^* \geq 0$ such that $B_k + \sigma^* I$ is positive semi-definite with*

$$(B_k + \sigma^* I)p^* = -g_k, \quad \sigma^*(\delta_k - \|p^*\|_2) = 0. \quad (9)$$

Moreover, if $B_k + \sigma^ I$ is positive definite, then the global minimizer is unique.*

In the following sections, we provide a comprehensive description of the two considered QN methods in a TR framework named L-BFGS-TR and L-SR1-TR to solve the DL optimization problem (1). In both methods, using the computed search direction $p_k \triangleq p^*$, the current iterate w_k is updated by (6). According to the step-acceptance condition based on the value of (8) for the computed p_k , the step may be accepted or rejected. In the latter case, the subproblem (7) is solved again for p_k after shrinking δ_k . The process of adjustment of the TR radius at each iteration of this method is described in Algorithm 6 in Appendix Appendix C.

3. The L-BFGS-TR method

BFGS is the most popular QN update in Broyden class, that is, which provides a Hessian approximation B_k for which (4) holds. It has the following general form

$$B_{k+1} = B_k - \frac{B_k s_k s_k^T B_k}{s_k^T B_k s_k} + \frac{y_k y_k^T}{y_k^T s_k}, \quad k = 0, 1, \dots, \quad (10)$$

which is a positive definite matrix, i.e., $B_{k+1} \succ 0$ if $B_0 \succ 0$ and the *curvature condition* holds, i.e., $s_k^T y_k > 0$. The difference between the symmetric approximations B_k and B_{k+1} is a rank-two matrix. In this work, we skip updating B_k if the following curvature condition is not satisfied for $\tau = 10^{-2}$:

$$s_k^T y_k > \tau \|s_k\|^2. \quad (11)$$

For large-scale optimization problems, using the limited-memory BFGS (L-BFGS) would be more efficient. In practice, only a collection of the most recent pairs $\{s_j, y_j\}$ is stored in memory, say l pairs, where $l \ll n$ (usually $l < 100$). In fact, for $k \geq l$, the l recent computed pairs are stored in the following matrices S_k and Y_k

$$S_k \triangleq [s_{k-l} \quad s_{k-(l-1)} \quad \dots \quad s_{k-1}], \quad Y_k \triangleq [y_{k-l} \quad y_{k-(l-1)} \quad \dots \quad y_{k-1}]. \quad (12)$$

Using (12), the L-BFGS matrix B_k can be represented in the following compact form

$$B_k = B_0 + \Psi_k M_k \Psi_k^T, \quad k = 1, 2, \dots, \quad (13)$$

where $B_0 = \gamma_k I \succ 0$ and

$$\Psi_k = [B_0 S_k \quad Y_k], \quad M_k = \begin{bmatrix} -S_k^T B_0 S_k & -L_k \\ -L_k^T & D_k \end{bmatrix}^{-1}. \quad (14)$$

We note that Ψ_k and M_k have at most $2l$ columns. In (14), matrices L_k , U_k and D_k are, respectively, the strictly lower triangular part, the strictly upper triangular part and the diagonal part of the following matrix splitting

$$S_k^T Y_k = L_k + D_k + U_k. \quad (15)$$

In order to solve the trust-region subproblem (7), where the Hessian approximation B_k is in the compact form, we used the procedure described in [1, 10, 39]; see [Algorithm 4](#) in [Appendix Appendix C](#).

One issue in QN algorithms is how to choose the initial Hessian approximation B_0 . Matrix B_0 is often set to some multiple of the identity matrix $B_0 = \gamma_k I$. A heuristic and conventional method to choose this multiple is

$$\gamma_k = \frac{y_{k-1}^T y_{k-1}}{y_{k-1}^T s_{k-1}} \triangleq \gamma_k^h. \quad (16)$$

The quotient of (16) is an approximation to an eigenvalue of $\nabla^2 F(w_k)$ and appears to be the most successful choice in practice [38]. Obviously, the selection of γ_k is important in generating Hessian approximations B_k . However, in DL optimization (1) where the true Hessian might

be indefinite, the positive definite L-BFGS B_k has a difficult task to approximate it. Here, the choice of γ_k would also be crucial for a second reason. In fact, according to [17, 39], an extra condition can be imposed on γ_k to avoid false negative curvature information, i.e., to avoid $p_k^T B_k p_k < 0$ whenever $p_k^T \nabla^2(w_k) p_k > 0$. Let, for simplicity, the objective function of (1) be a quadratic function

$$F(w) = \frac{1}{2} w^T H w + g^T w, \quad (17)$$

where $H = \nabla^2 F(w)$ which results in $\nabla F(w_{k+1}) - \nabla F(w_k) = H(w_{k+1} - w_k)$, and thus $y_k = H s_k$ for all k . By that, we have $S_k^T Y_k = S_k^T H S_k$. For the quadratic model and using (3), we have

$$S_k^T H S_k - \gamma_k S_k^T S_k = S_k^T \Psi_k M_k \Psi_k^T S_k. \quad (18)$$

According to (18), if H is not positive definite, then its negative curvature information can be captured by $S_k^T \Psi_k M_k \Psi_k^T S_k$ as $\gamma_k > 0$. However, false curvature information can be produced when γ_k is chosen too big while H is positive definite. To avoid this, γ_k is selected in $(0, \hat{\lambda})$ where $\hat{\lambda}$ is the smallest eigenvalue of the following generalized eigenvalue problem:

$$(L_k + D_k + L_k^T)u = \lambda S_k^T S_k u, \quad (19)$$

with L_k and D_k defined in (15). If $\hat{\lambda} \leq 0$, then γ_k is the maximum value of 1 and γ_k^h defined in (16); see Algorithm 8 in Appendix Appendix C. A detailed algorithm of the L-BFGS-TR method for solving the DL optimization problem (1) is outlined in Algorithm 7 in Appendix Appendix C.

4. The L-SR1-TR method

Another popular QN update in the Broyden class is the SR1 formula which generates good approximations to the true Hessian matrix, often better than the BFGS approximations [38]. We would like to determine whether better training results could be achieved by using these updates as they allow for indefinite Hessian approximations.

The SR1 updating formula verifying the secant equation (4) is given by

$$B_{k+1} = B_k + \frac{(y_k - B_k s_k)(y_k - B_k s_k)^T}{(y_k - B_k s_k)^T s_k}, \quad k = 0, 1, \dots \quad (20)$$

In this case, the difference between the symmetric approximations B_k and B_{k+1} is a rank-one matrix. Unlike (10), if B_k is positive definite, B_{k+1} may have not the same property. Regardless of the sign of $y_k^T s_k$ for each k , the SR1 method generates a sequence of matrices that may be indefinite. We note that the value of the quadratic model in (7) evaluated at the descent direction p^* is always smaller if this direction is also a direction of negative curvature. Therefore, the ability to generate indefinite approximations can actually be regarded as one of chief advantages of SR1 updates in non-convex settings like in DL applications.

To prevent vanishing of the denominator in (20), a simple safeguard which performs well in practice is simply skipping the update if the denominator is small [38]; i.e., $B_{k+1} = B_k$. Therefore, the update (20) is applied only if

$$|s^T(y_k - B_k s_k)| \geq \tau \|s_k\| \|y_k - B_k s_k\|, \quad (21)$$

where $\tau \in (0, 1)$ is small, say $\tau = 10^{-8}$.

In the limited-memory version of the SR1 (denoted by L-SR1) update, as in L-BFGS, only the l most recent curvature pairs are stored in matrices S_k and Y_k defined in (12). Using S_k and Y_k , the L-SR1 matrix B_k can be represented in the following compact form

$$B_k = B_0 + \Psi_k M_k \Psi_k^T, \quad k = 1, 2, \dots, \quad (22)$$

where $B_0 = \gamma_k I$ for some $\gamma_k \neq 0$ and

$$\Psi_k = Y_k - B_0 S_k, \quad M_k = (D_k + L_k + L_k^T - S_k^T B_0 S_k)^{-1}. \quad (23)$$

In (23), L_k and D_k are, respectively, the strictly lower triangular part and the diagonal part of $S_k^T Y_k$. We note that Ψ_k and M_k in the L-SR1 update have at most l columns.

To solve (7) where B_k is a L-SR1 Hessian approximation in compact form (22), we used the algorithm called the *Orthonormal Basis L-SR1* (OBS) proposed in [10]; a description of this procedure is given in Algorithm 5.

In [17], it was proven that the trust-region subproblem solution becomes closely parallel to the eigenvector corresponding to the most negative eigenvalue of the L-SR1 approximation B_k . This shows the importance of B_k to be able to capture curvature information correctly. On the other hand, it was highlighted how the choice of $B_0 = \gamma_k I$ affects B_k ; in fact, not choosing γ_k judiciously in relation to $\hat{\lambda}$ as the smallest eigenvalue of (19) can have adverse effects. Selecting $\gamma_k > \hat{\lambda}$ can result in false curvature information. Moreover, if γ_k is too close to $\hat{\lambda}$ from below, then B_k becomes ill-conditioned. If γ_k is too close to $\hat{\lambda}$ from above, then the smallest eigenvalue of B_k becomes negatively large arbitrarily. According to [17], the following lemma suggests selecting γ_k near but strictly less than $\hat{\lambda}$ to avoid asymptotically poor conditioning while improving the negative curvature approximation properties of B_k .

Lemma 4.1. *For a given quadratic objective function (17), let $\hat{\lambda}$ denote the smallest eigenvalue of the generalized eigenvalue problem (19). Then for all $\gamma_k < \hat{\lambda}$, the smallest eigenvalue of B_k is bounded above by the smallest eigenvalue of H in the span of S_k , i.e.*

$$\lambda_{\min}(B_k) \leq \min_{S_k v \neq 0} \frac{v^T S_k^T H S_k v}{v^T S_k^T S_k v}.$$

In this work, we set $\gamma_k = \max\{10^{-6}, 0.5\hat{\lambda}\}$ in the case where $\hat{\lambda} > 0$; otherwise the γ_k is set to $\gamma_k = \min\{-10^{-6}, 1.5\hat{\lambda}\}$; see Algorithm 10 in Appendix C. A detailed algorithm of the L-SR1-TR method for solving the DL problem (1) is given in Algorithm 9.

5. Subsampling strategies and stochastic algorithms

The main motivation behind the use of stochastic optimization algorithms in deep learning may be traced back to the existence of a special type of redundancy due to similarity between data points in (1). Besides, the computation of the true gradient is expensive and the computation of the true Hessian is not practical in large-scale DL problems. Indeed, depending on the available computing resources, it could take a prohibitive amount of time to process the whole set of data examples as a single batch at each iteration of a deterministic algorithm. That is why most of the optimizers in DL work in the stochastic regime. In this

regime, the training set $\{(x_i, y_i)_{i=1}^N\}$ is divided randomly into multiple, say \bar{N} , batches. Then a stochastic algorithm uses a single batch J_k at iteration k to compute the required quantities, i.e., stochastic loss and stochastic gradient as follows

$$f_k^{J_k} \triangleq F^{J_k}(w_k) = \frac{1}{|J_k|} \sum_{i \in J_k^{idx}} L_i(w_k), \quad g_k^{J_k} \triangleq \nabla F^{J_k}(w_k) = \frac{1}{|J_k|} \sum_{i \in J_k^{idx}} \nabla L_i(w_k), \quad (24)$$

where $bs \triangleq |J_k|$ and J_k^{idx} denote the size of J_k and the index set of the samples belonging to J_k , respectively. In other words, the stochastic QN (sQN) extensions are obtained by replacement of the full loss f_k and gradient g_k in (2) with $f_k^{J_k}$ and $g_k^{J_k}$, respectively, throughout the iterative process of the algorithms. The process of randomly taking J_k , computing the required quantities (24) for finding a search direction and then updating w_k constitutes one single iteration of a stochastic algorithm. This process is repeated for a given number of batches till one epoch (i.e. one pass through the whole set of data samples) is completed. At that point, the dataset is shuffled and new batches are generated for the next epoch; see Algorithm 1 and Algorithm 2 for a description of the stochastic variants of L-BFGS-TR and L-SR1-TR algorithms, respectively.

5.1. Sampling strategy and batch formation

In a stochastic setting, since batches change from one iteration to the next, differences in stochastic gradients can cause the updating process to yield poor curvature estimates (s_k, y_k) . Therefore, updating B_k whether as (3) or (22) may lead to unstable Hessian approximations. In order to address this issue, the following approaches have been proposed in literature:

- As a primary remedy [42], one can use the same batch J_k for computing curvature pairs as follows

$$(s_k, y_k) = (p_k, g_t^{J_k} - g_k^{J_k}), \quad (25)$$

where $g_t^{J_k} \triangleq \nabla F^{J_k}(w_t)$. We refer to this strategy as full-batch sampling. In this strategy the stochastic gradient at w_t is computed twice: one in (25) and another to compute the subsequent step, i.e., $g_t^{J_{k+1}}$ if w_t is accepted; otherwise $g_k^{J_{k+1}}$ is computed.

- As a cheaper alternative, an overlap sampling strategy was proposed in [3] in which only a common (overlapping) part between every two consecutive batches J_k and J_{k+1} is employed for computing y_k . Defining $O_k = J_k \cap J_{k+1} \neq \emptyset$ of size $os \triangleq |O_k|$, the curvature pairs are computed as

$$(s_k, y_k) = (p_k, g_t^{O_k} - g_k^{O_k}), \quad (26)$$

where $g_t^{O_k} \triangleq \nabla F^{O_k}(w_t)$. Since O_k , and thus J_k , should be *sizeable*, this strategy is called multi-batch sampling.

Both these approaches were originally considered for a stochastic algorithm using L-BFGS updates without and with line search method, respectively. Progressive sampling approaches to use L-SR1 updates in a TR framework were instead considered to train fully connected networks in [17, 45]. More precisely, in [17], the curvature pairs and the model goodness ratio are computed as

$$(s_k, y_k) = (p_k, g_t^{J_k} - g_k^{J_k}), \quad \rho_k = \frac{f_t^{J_k} - f_k^{J_k}}{Q_k(p_k)}. \quad (27)$$

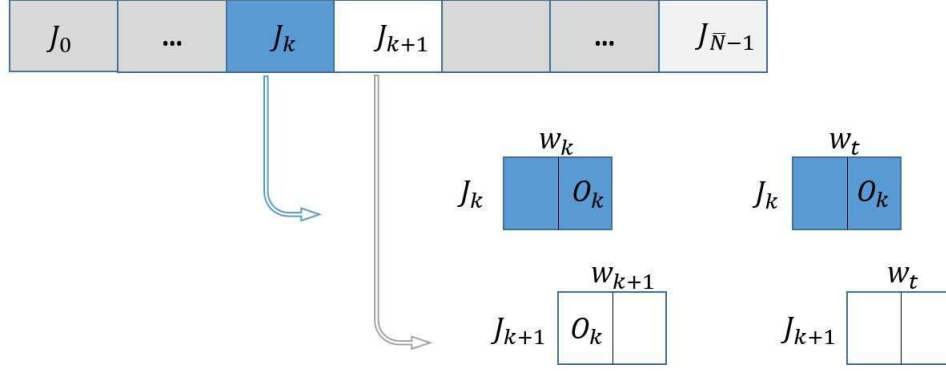


Figure 1 Fixed size batches strategy scheme.

where $g_t^{O_k} \triangleq \nabla F^{O_k}(w_t)$, $f_t^{O_k} \triangleq F^{O_k}(w_t)$ and $J_k = J_k \cap J_{k+1}$. Although progressive sampling strategies may avoid getting noisy gradients by increasing the batch size at each iteration [7], they also increase the iteration cost.

We have examined the following two strategies to implement the considered sQN methods in a TR approach in which the subsampled function and gradient evaluations are computed using a fixed size batch per iteration. Let $O_k = J_k \cap J_{k+1} \neq \emptyset$; then

- **Option 1.** $(s_k, y_k) = (p_k, g_t^{J_k} - g_k^{J_k})$, $\rho_k = \frac{f_t^{J_k} - f_k^{J_k}}{Q_k(p_k)}$.
- **Option 2.** $(s_k, y_k) = (p_k, g_t^{O_k} - g_k^{O_k})$, $\rho_k = \frac{f_t^{O_k} - f_k^{O_k}}{Q_k(p_k)}$.

Clearly, in both options, every two successive batches have an overlapping set (O_k) which helps to avoid extra computations in the subsequent iteration. We have performed experiments with both sampling strategies and found that the L-SR1 algorithm failed to converge when using the second option. Since this fact deserves further investigation, we have only used the first sampling option in this paper.

The fixed size batches are drawn without replacement to be sure about one pass through whole data in one epoch. Let $J_k = O_{k-1} \cup O_k$ where O_{k-1} and O_k are the overlapping samples of J_k with batches J_{k-1} and J_{k+1} , respectively. We assume that $|O_{k-1}| = |O_k| = os$ and thus overlap ratio $or \triangleq \frac{os}{bs} = \frac{1}{2}$ (half overlapping). It is easy to see that $\bar{N} = \left\lfloor \frac{N}{os} \right\rfloor - 1$ indicates the number of batches in one epoch, where $\lfloor a \rfloor$ rounds a to the nearest integer less than or equal to a . To create \bar{N} batches, we consider the two following cases:

- **Case 1.** $rs \triangleq \text{mod}(N, os) = 0$,
- **Case 2.** $rs \triangleq \text{mod}(N, os) \neq 0$,

where the mod (modulo operation) of N and os returns the remainder after division of N and os . In the first case, all \bar{N} batches are duplex created by two subsets O_{k-1} and O_k as $J_k = O_{k-1} \cup O_k$ while in the second case, the \bar{N} th batch is a triple batch as $J_k = O_{k-1} \cup R_k \cup O_k$ where R_k is a subset of size $rs \neq 0$ and other $\bar{N} - 1$ batches are duplex; see Algorithm 3.

Algorithm 1 Stochastic trust-region L-BFGS (sL-BFGS-TR)

```
1: Inputs:  $w_0 \in \mathbb{R}^n$ ,  $\epsilon > 0$ ,  $os$ ,  $\text{epoch}_{max}$ ,  $l$ ,  $\gamma_0 > 0$ ,  $S_0 = Y_0 = [\cdot]$ ,  $0 < \tau, \tau_1 < 1$ 
2: for  $k = 0, 1, \dots$  do
3:   Take a random and uniform multi-batch  $J_k$  of size  $bs$  and compute  $f_k^{J_k}, g_k^{J_k}$  by (24)
4:   if  $\|g_k^{J_k}\| \leq \epsilon$  or  $\text{epoch} > \text{epoch}_{max}$  then
5:     Stop training
6:   end if
7:   Compute  $p_k$  using Algorithm 4
8:   Compute  $w_t = w_k + p_k$  and  $f_t^{J_k}, g_t^{J_k}$  by (24)
9:   Compute  $(s_k, y_k) = (w_t - w_k, g_t^{J_k} - g_k^{J_k})$  and  $\rho_k = \frac{f_t^{J_k} - f_k^{J_k}}{Q(p_k)}$ 
10:  if  $\rho_k \geq \tau_1$  then
11:     $w_{k+1} = w_t$ 
12:  else
13:     $w_{k+1} = w_k$ 
14:  end if
15:  Update  $\delta_k$  by Algorithm 6
16:  if  $s_k^T y_k > \tau \|s_k\|^2$  then
17:    Update storage matrices  $S_{k+1}$  and  $Y_{k+1}$  by  $l$  recent  $\{s_j, y_j\}_{j=k-l+1}^k$ 
18:    Compute  $\gamma_{k+1}$  for  $B_0$  by Algorithm 8 and  $\Psi_{k+1}, M_{k+1}^{-1}$  by (3)
19:  else
20:    Set  $\gamma_{k+1} = \gamma_k$ ,  $\Psi_{k+1} = \Psi_k$  and  $M_{k+1}^{-1} = M_k^{-1}$ 
21:  end if
22: end for
```

In Case 1, the required quantities for computing y_k and ρ_k in Option 1 at iteration k are determined by

$$f_k^{J_k} = or(f_k^{O_{k-1}} + f_k^{O_k}), \quad g_k^{J_k} = or(g_k^{O_{k-1}} + g_k^{O_k}), \quad (28)$$

where $or = \frac{1}{2}$. In case 2, the required quantities with respect to the last triple batch $J_k = O_{k-1} \cup R_k \cup O_k$ are computed by

$$f_k^{J_k} = or(f_k^{O_{k-1}} + f_k^{O_k}) + (1 - 2or)f_k^{R_k}, \quad g_k^{J_k} = or(g_k^{O_{k-1}} + g_k^{O_k}) + (1 - 2or)g_k^{R_k}, \quad (29)$$

where $or = \frac{os}{2os + rs}$. In this work, we have considered batches corresponding to case 1.

Figure 1 schematically shows batches J_k and J_{k+1} at iterations k and $k+1$, respectively, and the overlapping parts in case 1. The stochastic loss value and gradient (28) are computed at the beginning (at w_k) and at the end of each iteration (at trial point w_t). In iteration $k+1$, these quantities have to be evaluated with respect to the sample subset represented by white rectangles only. In fact, the computations with respect to subset O_k at w_{k+1} depend on the acceptance status of w_t at iteration k . In case of acceptance, the loss function and gradient vector have been already computed at w_t ; in case of rejection, these quantities are set equal to those evaluated at w_k with respect to subset O_k . Detailed versions of Algorithm 1 and Algorithm 2 are respectively provided in Algorithm 11 and Algorithm 12 in Appendix Appendix C.

6. Empirical study

We present in this section the results of an extensive experimentation with the two described stochastic QN algorithms on image classification problems, using three well established data sets. In order to find an optimal classification model by using a C -class

Algorithm 2 Stochastic trust-region L-SR1 (sL-SR1-TR)

```

1: Inputs:  $w_0 \in \mathbb{R}^n$ ,  $\epsilon > 0$ ,  $os$ ,  $\text{epoch}_{max}$ ,  $l$ ,  $\gamma_0 > 0$ ,  $S_0 = Y_0 = [\cdot]$ ,  $0 < \tau, \tau_1 < 1$ 
2: for  $k = 0, 1, \dots$  do
3:   Take a random and uniform multi-batch  $J_k$  of size  $bs$  and compute  $f_k^{J_k}$ ,  $g_k^{J_k}$  by (24)
4:   if  $\|g_k^{J_k}\| \leq \epsilon$  or  $\text{epoch} > \text{epoch}_{max}$  then
5:     Stop training
6:   end if
7:   Compute  $p_k$  using Algorithm 5
8:   Compute  $w_t = w_k + p_k$  and  $f_t^{J_k}$ ,  $g_t^{J_k}$  by (24)
9:   Compute  $(s_k, y_k) = (w_t - w_k, g_t^{J_k} - g_k^{J_k})$  and  $\rho_k = \frac{f_t^{J_k} - f_k^{J_k}}{Q(p_k)}$ 
10:  if  $\rho_k \geq \tau_1$  then
11:     $w_{k+1} = w_t$ 
12:  else
13:     $w_{k+1} = w_k$ 
14:  end if
15:  Update  $\delta_k$  by Algorithm 6
16:  if  $|s^T(y_k - B_k s_k)| \geq \tau \|s_k\| \|y_k - B_k s_k\|$  then
17:    Update storage matrices  $S_{k+1}$  and  $Y_{k+1}$  by  $l$  recent  $\{s_j, y_j\}_{j=k-l+1}^k$ 
18:    Compute  $\gamma_{k+1}$  for  $B_0$  by Algorithm 10 and  $\Psi_{k+1}$ ,  $M_{k+1}^{-1}$  by (23)
19:  else
20:    Set  $\gamma_{k+1} = \gamma_k$ ,  $\Psi_{k+1} = \Psi_k$  and  $M_{k+1}^{-1} = M_k^{-1}$ 
21:  end if
22: end for

```

dataset, the generic problem (1) is solved by employing the *softmax cross-entropy* function $L_i(w) = -\sum_{i=1}^C (y_i)_k \log(h(x_i; w))_k$ for $i = 1, \dots, N$.

One of the most popular benchmarks to make informed decisions using data-driven approaches in DL is the MNIST dataset [29] as $\{(x_i, y_i)_{i=1}^{70000}\}$ consisting in handwritten gray-scale images of digits x_i with 28×28 pixels taken values in $[0, 255]$ and its corresponding labels converted to one-hot vectors. The Fashion-MNIST [46] is a variant of the original MNIST dataset which shares the same image size and structure. Its images are assigned to fashion items (clothing) belonging also to 10 classes but working with this dataset is more challenging than working with MNIST. The CIFAR-10 dataset [27] has 60000 RGB images x_i of 32×32 pixels taken values in $[0, 255]$ in 10 classes. Every single image of MNIST and Fashion-MNIST datasets is $x_i \in \mathbb{R}^{28 \times 28 \times 1}$ while one of CIFAR10 is $x_i \in \mathbb{R}^{32 \times 32 \times 3}$. In all datasets, 10000 of the images are set aside as testing set. We use them as validation set during training.

The Deep Learning Toolbox of MATLAB provides a framework for designing and implementing a deep neural network to perform image classification task using a prescribed training algorithm. Since the algorithms considered in this work, sL-BFGS-TR and sL-SR1-TR, are not defined as built-in functions, we have exploited the Deep Learning Custom Training Loops of MATLAB¹ to implement them according to the algorithms described in Algorithm 11 and Algorithm 12, respectively. All the hyper-parameters associated to these methods have been included in the description of the algorithms. Implementation details of the two stochastic QN algorithms considered in this work using the DL toolbox of MATLAB² are provided

¹<https://www.mathworks.com/help/deeplearning/deep-learning-custom-training-loops.html>

²<https://it.mathworks.com/help/deeplearning/>

in https://github.com/MATHinDL/sL_QN_TR/ where all the codes employed to obtain the numerical results included in this paper are also available.

In the following subsections we describe the architectures and the experimental setup.

6.1. Networks architecture

Convolutional neural networks (CNNs) are the most popular types of DNNs. They are arranged according to a spatial grid data structure with strong spatial dependencies such as images. For image classification tasks a large variety of CNNs architectures with different number of fully connected (FC) layers at the end of their structure have been proposed and tested in the literature. In this work, inspired by LeNet-5 mainly used for character recognition tasks [30], we have used a LeNet-like network with a shallow structure. We have also employed a modern ResNet-20 residual network [22] exploiting special skip connections (shortcuts) to avoid possible gradient vanishing that might happen due to its deep architecture. Finally, we also consider a self-built CNN named ConvNet3FC2 with larger number of parameters than the two previous networks. Table 1 describes the networks' architecture in detail. To analyze the effect of batch normalization [23] on the performance of the stochastic QN algorithms, we have considered also variants of ResNet-20 and ConvNet3FC2 networks, named ResNet-20(no BN) and ConvNet3FC2(no BN), in which the batch normalization layers have been removed.

6.2. Experiments

We have compared sL-BFGS-TR and sL-SR1-TR in image classification problems using the previously described standard datasets to train the DNN for at most 10 epochs. Table 2 shows the total number of trainable parameters, n , for each problem.

We have performed extensive testing to analyze different aspects that may influence the performance of the two considered stochastic QN algorithms, mainly, the limited memory parameter and the batch size. We have also analyzed the performance of both the algorithms of interest from the point of view of CPU time and, finally, we have provided a comparison with a popular first order method. We have analyzed all these aspects with and without the employment of batch normalization layers.

To evaluate the performance of a model (network) in classification of data belonging to C classes with balanced number of samples, measuring accuracy is typically considered. The accuracy is the ratio of the number of correct predictions to the number of total predictions. In our study, we report the accuracy in percentage and overall loss values for both train and test (validation) datasets. In the Figures reporting the results of the experiments, to allow for a better visualization, we have shown measurements of evaluation versus epochs using a determined frequency of display reported at the top of the figures. Display frequency values larger than one indicate the number of iterations which are not reported while all the iterations are considered if the display frequency is one.

All experiments were performed with the MATLAB DL toolbox on an Ubuntu Linux server virtual machine with 32 CPUs and 128GB RAM. In all the experiments, we show results of a single run as the performance of the methods of interest did not vary significantly. We used the same initial parameter $w_0 \in \mathbb{R}^n$ by specifying the same seed to the MATLAB random number generator.

LeNet-like	
Structure	$(Conv(5 \times 5@20, 1, 0)/ReLU/MaxPool(2 \times 2, 2, 0))$
	$(Conv(5 \times 5@50, 1, 0)/ReLU/MaxPool(2 \times 2, 2, 0))$
	$FC(500/ReLU)$
	$FC(C/Softmax)$
ResNet-20	
Structure	$(Conv(3 \times 3@16, 1, 1)/BN/ReLU)$
	$B_1 \left\{ \begin{array}{l} (Conv(3 \times 3@16, 1, 1)/BN/ReLU) \\ (Conv(3 \times 3@16, 1, 1)/BN) + addition(1)/Relu \end{array} \right.$
	$B_2 \left\{ \begin{array}{l} (Conv(3 \times 3@16, 1, 1)/BN/ReLU) \\ (Conv(3 \times 3@16, 1, 1)/BN) + addition(1)/Relu \end{array} \right.$
	$B_3 \left\{ \begin{array}{l} (Conv(3 \times 3@16, 1, 1)/BN/ReLU) \\ (Conv(3 \times 3@16, 1, 1)/BN) + addition(1)/Relu \end{array} \right.$
	$B_1 \left\{ \begin{array}{l} (Conv(3 \times 3@32, 2, 1)/BN/ReLU) \\ (Conv(3 \times 3@32, 1, 1)/BN) \\ (Conv(1 \times 1@32, 2, 0)/BN) + addition(2)/Relu \end{array} \right.$
	$B_2 \left\{ \begin{array}{l} (Conv(3 \times 3@32, 1, 1)/BN/ReLU) \\ (Conv(3 \times 3@32, 1, 1)/BN) + addition(1)/Relu \end{array} \right.$
	$B_3 \left\{ \begin{array}{l} (Conv(3 \times 3@32, 1, 1)/BN/ReLU) \\ (Conv(3 \times 3@32, 1, 1)/BN) + addition(1)/Relu \end{array} \right.$
	$B_1 \left\{ \begin{array}{l} (Conv(3 \times 3@64, 2, 1)/BN/ReLU) \\ (Conv(3 \times 3@64, 1, 1)/BN) \\ (Conv(1 \times 1@64, 2, 0)/BN) + addition(2)/Relu \end{array} \right.$
	$B_2 \left\{ \begin{array}{l} (Conv(3 \times 3@64, 1, 1)/BN/ReLU) \\ (Conv(3 \times 3@64, 1, 1)/BN) + addition(1)/Relu \end{array} \right.$
	$B_3 \left\{ \begin{array}{l} (Conv(3 \times 3@64, 1, 1)/BN/ReLU) \\ (Conv(3 \times 3@64, 1, 1)/BN) + addition(1)/g.AvgPool/ReLU \end{array} \right.$
	$FC(C/Softmax)$
ConvNet3FC2	
Structure	$(Conv(5 \times 5@32, 1, 2)/BN/ReLU/MaxPool(2 \times 2, 1, 0))$
	$(Conv(5 \times 5@32, 1, 2)/BN/ReLU/MaxPool(2 \times 2, 1, 0))$
	$(Conv(5 \times 5@64, 1, 2)/BN/ReLU/MaxPool(2 \times 2, 1, 0))$
	$FC(64, /BN/ReLU)$
	$FC(C/Softmax)$

Table 1 Networks.

In this table,

- the syntax $(Conv(5 \times 5@32, 1, 2)/BN/ReLU/MaxPool(2 \times 2, 1, 0))$ indicates a simple convolutional network (convnet) including a convolutional layer ($Conv$) using 32 filters of size 5×5 , stride 1, padding 2, followed by a batch normalization layer (BN), a nonlinear activation function ($ReLU$) and, finally, a max-pooling layer with a channel of size 2×2 , stride 1 and padding 0.
- the syntax $FC(C/Softmax)$ indicates a layer of C fully connected neurons followed by the *softmax* layer.
- the syntax $addition(1)/Relu$ indicates the existence of an *identity shortcut* with functionality such that the output of a given block, say B_1 (or B_2 or B_3), is directly fed to the *addition* layer and then to the $ReLU$ layer while $addition(2)/Relu$ in a block shows the existence of a *projection shortcut* by which the output from the two first convnets is added to the output of the third convnet and then the output is passed through the $ReLU$ layer.

	LeNet-5	ResNet-20	ResNet-20(no BN)	ConvNet3FC2	ConvNet3FC2(no BN)
MNIST	431,030	272,970	271,402	2,638,826	2,638,442
F.MNIST	431,030	272,970	271,402	2,638,826	2,638,442
CIFAR10	657,080	273,258	271,690	3,524,778	3,525,162

Table 2 The total number of networks’ trainable parameters (n).

	LeNet-like	ResNet-20	ResNet-20(no BN)	ConvNet3FC2	ConvNet3FC2(no BN)
MNIST	Figure 3 Figure 8*	-	-	Figure 3 Figure 14*	Figure 3 Figure 17*
F.MNIST	Figure 3 Figure 9*	Figure 3 Figure 10*	Figure 3 Figure 12*	Figure 3 Figure 15*	Figure 3 Figure 18*
CIFAR10	-	Figure 3 Figure 11*	Figure 3 Figure 13*	Figure 3 Figure 16*	Figure 3 Figure 19*

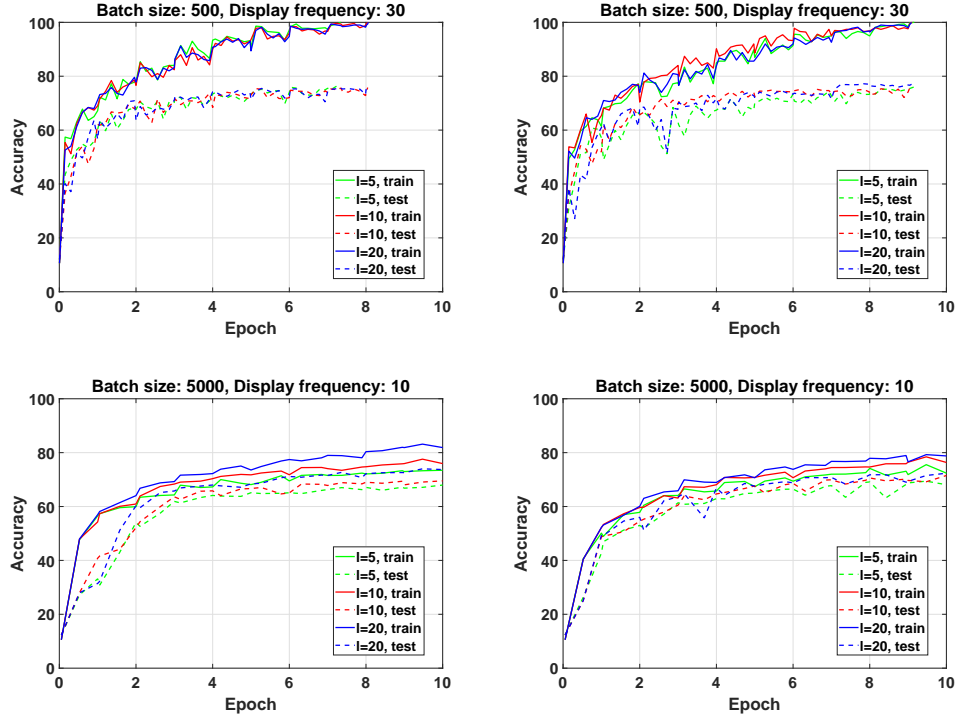
Table 3 Set of Figures corresponding to experiments in Section 6.2.2. Figures marked as * can be found in the supplementary material.

6.2.1. Influence of the limited memory parameter

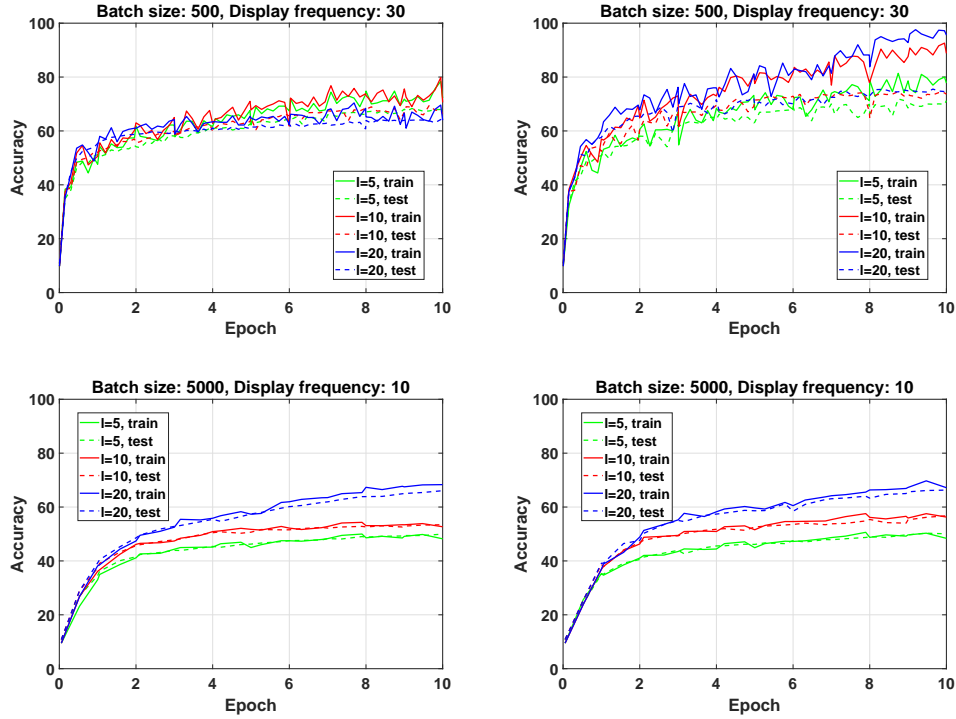
The results reported in Figure 2 illustrate the effect of the limited memory parameter value ($l = 5, 10$ and 20) on the accuracy achieved by the two stochastic QN algorithms to train ConvNet3FC2 on CIFAR10 within a fixed number of epochs. As it is clearly shown in this figure, in particular for ConvNet3FC2(no BN), the effect of the limited memory parameter is more pronounced when large batches are used ($bs = 5000$). For large batch sizes the larger the value of l the higher the accuracy. No remarkable differences on the behavior of both algorithms with small batch size ($bs = 500$) are observed. It seems that incorporating more recently computed curvature vectors (i.e. larger l) does not increase the efficiency of the algorithms to train DNNs with BN layers while it does when BN layers are removed. Finally, we remark that we found that using larger values of l ($l \geq 30$) was not helpful since it led to higher over-fitting in some of our experiments.

6.2.2. Influence of the batch size

In this subsection we analyze the effect of the batch size in the performance of the two considered sQN methods while keeping fixed the limited memory parameter $l = 20$. We have considered different values of the batch size (bs) in $\{100, 500, 1000, 5000\}$ or, equivalently, overlap size (os) in $\{50, 250, 500, 2500\}$ for all the problems and all the considered DNNs. The results of these experiments have been reported in Figure 3 (see also Figures 8–19 in the Supplementary Material). The general conclusion is that when training the networks for a fixed number of epochs, the achieved accuracy decreases when the batch size increases. This is due to the reduction in the number of parameter updates. We have summarized in Table 4 the relative superiority of one of the two stochastic QN algorithms over the other for all problems. This table indicates that sL-SR1-TR performs better than sL-BFGS-TR for training networks without BN layers while both QN updates exhibit comparable performances when used for training networks with BN layers. More detailed comments for each DNN are given below.



(a) *CIFAR10 with ConvNet3FC2*



(b) *CIFAR10 with ConvNet3FC2(no BN)*

Figure 2 Performance of *sL-BFGS-TR* (left) and *sL-SR1-TR* (right) with different limited memory values (l).

LeNet-like

The results on top of [Figure 3](#) (see also Figures 8 and 9) show that both algorithms perform well in training LeNet-like within 10 epochs to classify MNIST and Fashion-MNIST datasets, respectively. Specifically, sL-SR1-TR provides better accuracy than sL-BFGS-TR.

ResNet-20

[Figure 3](#) (see also Figures 10-13) shows that the classification accuracy on Fashion-MNIST increases when using ResNet-20 instead of LeNet-like, as expected. Regarding the performance of the two algorithms of interest, we see in Figures 10 and 11 that when BN is used both algorithms exhibit comparable performances. Nevertheless, we point out the fact that sL-BFGS-TR using $bs = 100$ achieves higher accuracy than sL-SR1-TR in less time. Unfortunately, this comes with some awkward oscillations in the testing (validation) curves. We attribute these oscillations to a sort of inconsistency between the updated parameters and the normalized features of the testing set samples. This is due to the fact that the inference step by testing samples is done using the updated parameters and the features which are normalized by the most recently computed moving average of mean and moving average of variance obtained by batch normalization layers in training phase [\[23\]](#).

The numerical results on ResNet-20 without BN layers confirm this assumption can be true. These results also show that sL-SR1-TR performs better than sL-BFGS-TR in this case. Note that the experiments on LeNet-like and ResNet-20 with and without BN layers show that sL-SR1-TR performs better than sL-BFGS-TR when batch normalization is not used, but as it can be clearly seen from the results, the elimination of BN layers causes a detriment of all methods performances.

ConvNet3FC2

The results of the experiments regarding this network are summarized in [Figure 3](#) (see also Figures 14–19). As in the ResNet-20 architecture, we observe also in this network some oscillations in test accuracy curves but with lower-amplitude variations. This might be due to the minor number of BN layers present in ConvNet3FC2. The experiments show that sL-BFGS-TR still produces better testing/training accuracy than sL-SR1-TR on CIFAR10 while both algorithms behave similarly on MNIST and Fashion-MNIST datasets. Besides, sL-BFGS-TR with $bs = 100$ within 10 epochs achieves the highest accuracy faster than sL-SR1-TR (see [Figure 3](#) (k)). The exact reason of the different behavior of the two stochastic QN algorithms with networks **not** employing BN layers is not completely clear and would deserve further investigation.

6.2.3. CPU timings analysis

In this experiment, we have run the training algorithms for a maximum budget of time indicated on the x -axis of [Figure 4](#) (see also Figures 20 and 21). The goal is to see which algorithm achieves the highest training accuracy faster than the other one within a fixed number of epochs. [Figure 4](#) shows that sL-SR1-TR trains faster with better accuracy than sL-BFGS-TR. We have also made a comparison of both algorithms using ConvNet3FC2 with and without BN layers. [Figure 4](#) shows that both algorithms behave comparably within the selected interval of time when BN layers are used. Nevertheless, sL-SR1-TR is faster than sL-BFGS-TR to pass 10 epochs even if it does not achieve higher training accuracy. sL-SR1-TR is also the clear winner for network models without BN layers such as ConvNet3FC2 (no BN).

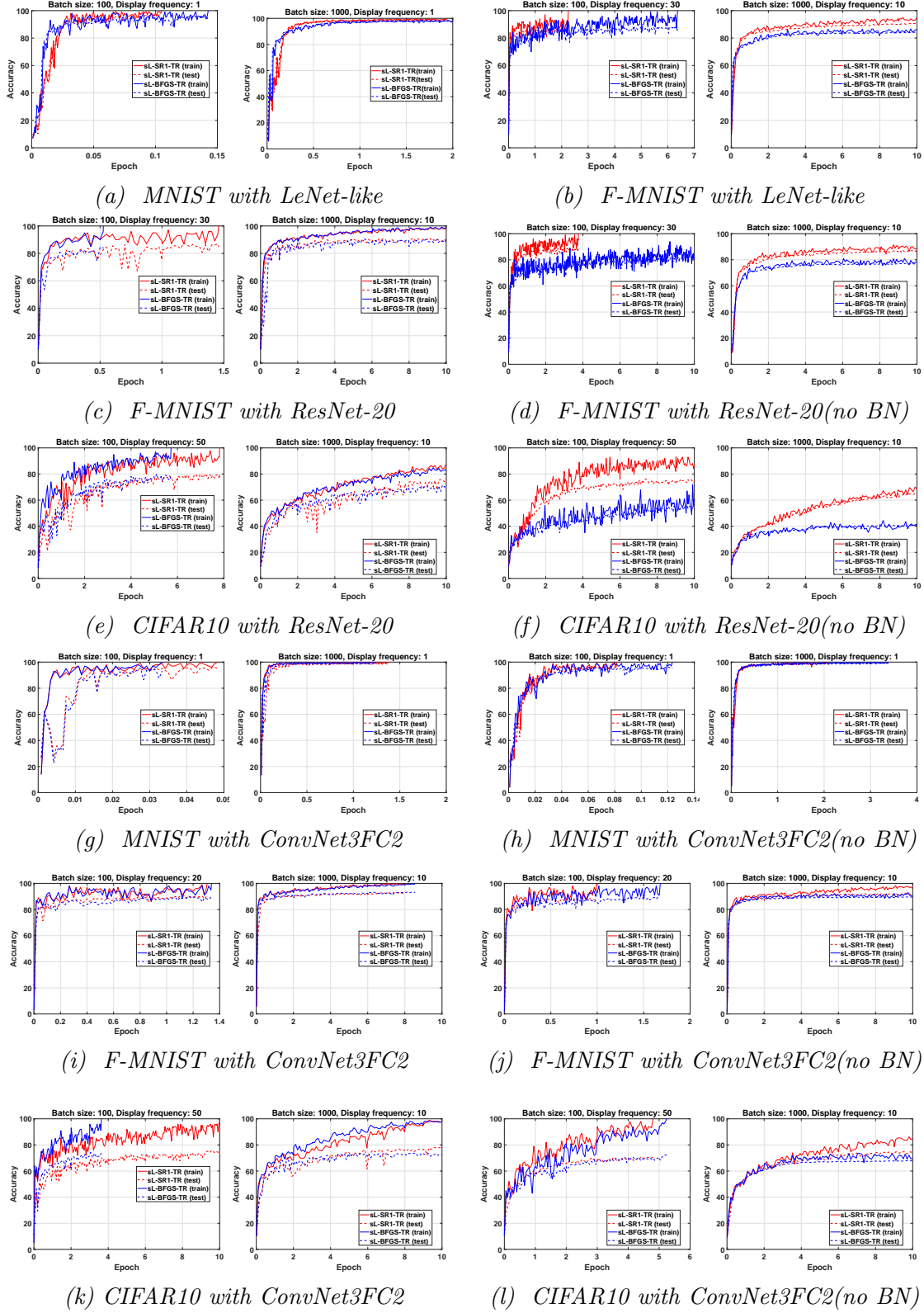


Figure 3 Evolution of the training and testing accuracy for batch sizes 100 and 1000 ($l = 20$).

	LeNet-5	ResNet-20	ResNet-20(no BN)	ConvNet3FC2	ConvNet3FC2(no BN)
MNIST	sL-SR1-TR	both	sL-SR1-TR	both	both
F.MNIST	sL-SR1-TR	both	sL-SR1-TR	both	sL-SR1-TR
CIFAR10	sL-SR1-TR	sL-BFGS-TR	sL-SR1-TR	sL-BFGS-TR	sL-SR1-TR

Table 4 Summary of the best sQN approach for each combination problem/network architecture.

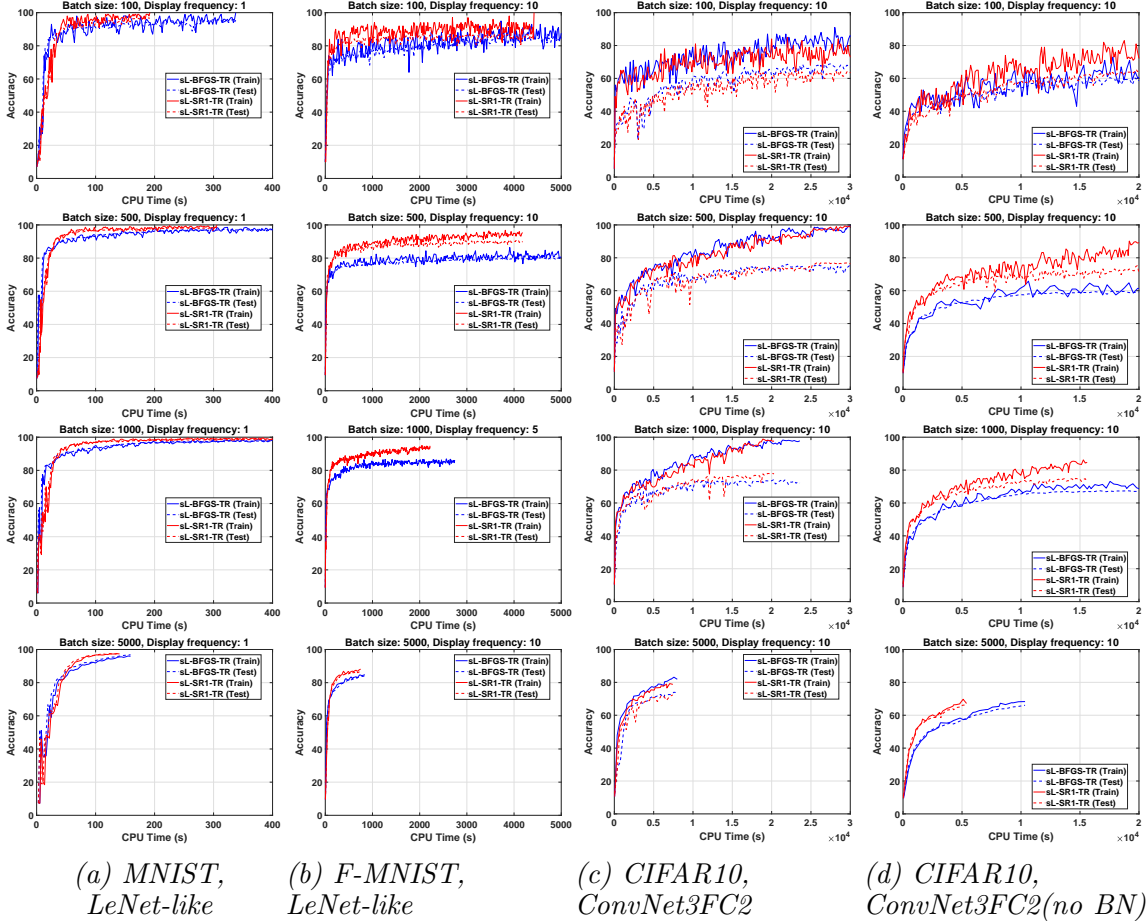


Figure 4 Training accuracy vs CPU time (in seconds) of both sQN algorithms with $l = 20$.

This experiment illustrates that both algorithms can yield very similar training accuracies regardless of the batch size. Despite of the small influence of the batch size on the final reached training and testing accuracy, it can be observed a slight increase in the accuracy when larger batch sizes are used. For this reason, one can prefer to employ larger batch sizes for sQN algorithms which can provide high benefit also in view of a parallel/distributed implementation.

Finally, it can be noted that based on the results of the experiments, sQN methods reveal very robust with respect to their hyper-parameters (limited memory parameter and batch size) and need minimal tuning.

6.2.4. Comparison with a progressive batching based algorithm

We have performed a comparison of our sQN training algorithms with algorithm STORM (Algorithm 2 in [13]). STORM relies on an adaptive batching strategy aimed to avoid inaccurate stochastic function evaluations in the TR framework. Note that the real reduction of the objective function is not guaranteed in a stochastic trust-region approach. In [13, 5], the authors claim that if the stochastic functions are sufficiently accurate, this will increase the number of true successful iterations. Therefore, they considered a progressive sampling strategy with sample size $b_k = \min(N, \max(b_0 * k + b_1, \lceil \frac{1}{\delta_k^2} \rceil))$ where δ_k is the trust-region radius at iteration k , N is total number of samples and b_0, b_1 are $b_0 = 100$, $b_1 = 32 \times 32 \times 3$ for CIFAR10 and $b_1 = 28 \times 28 \times 1$ for Fashion-MNIST. We have applied STORM with both SR1 and BFGS updates. We have compared the performances of sL-SR1-TR and sL-BFGS-TR algorithms with different overlapping batch sizes running for 10 epochs and STORM with progressive batch size b_k running for 50 epochs. The largest batch size reached by STORM was near $b_k = 25000$ (i.e., 50 percent of the total number of samples N). The results of this experiment are summarized in Figure 5. We notice that on all test cases the proposed stochastic quasi-Newton algorithms with fixed batch size yield comparable or better training and testing accuracy than the variance reduced³ STORM algorithm.

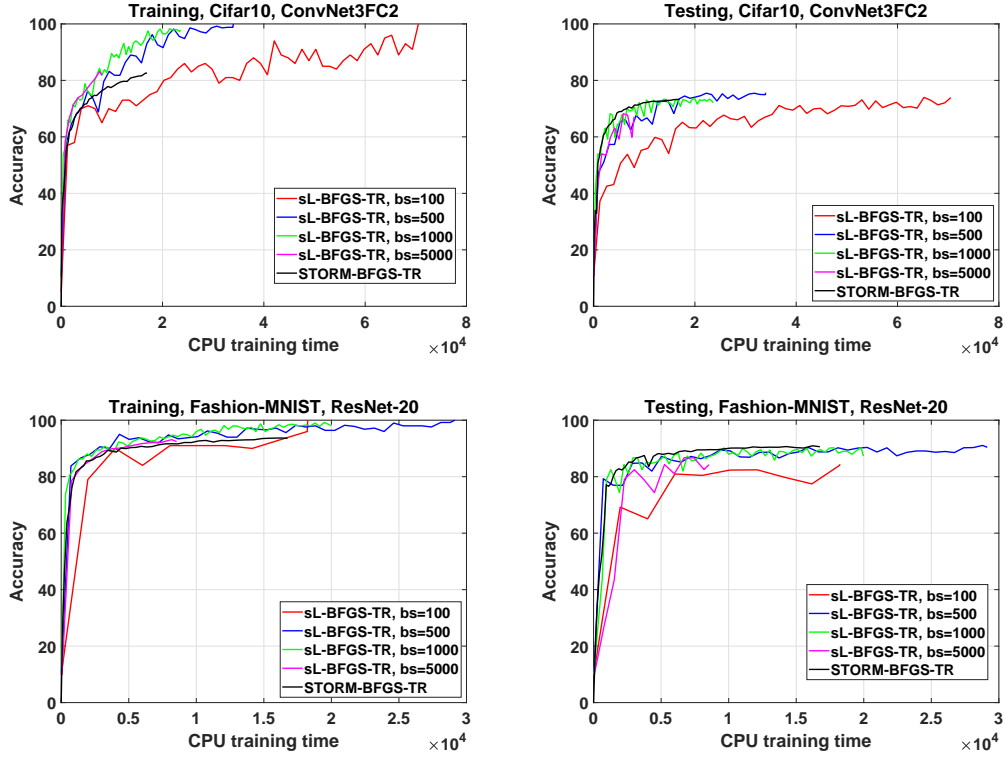
6.2.5. Comparison with Adam optimizer

Adaptive Moment Estimation (Adam) [26] is a popular efficient first-order optimizer used in DL. Due to the high sensitivity of Adam to the value of its hyper-parameters, it is usually used after the determination of near optimal values through grid searching strategies, which is a very time-consuming task. In order to compare sL-BFGS-TR and sL-SR1-TR against Adam we have performed a grid search onto learning rates and batch sizes to select the best value of Adam’s hyper-parameters. We consider learning rates values in $\{10^{-5}, 10^{-4}, 10^{-3}, 10^{-2}, 10^{-1}, 1\}$ and batch size in $\{100, 500, 1000, 5000\}$ and selected the values that allowed to achieve the highest testing accuracy. The gradient and squared gradient decay factors are set as $\beta_1 = 0.9$ and $\beta_2 = 0.999$, respectively. The small constant for preventing divide-by-zero errors is set to 10^{-8} .

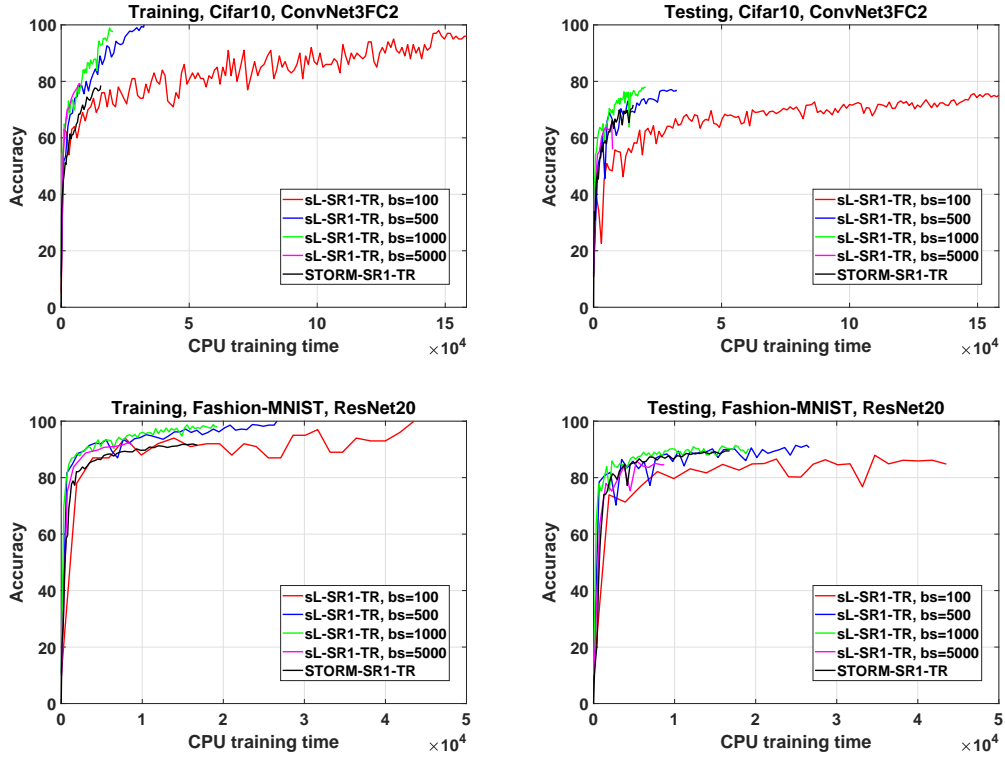
Figure 6 (see also Figures 22–26) illustrates the results obtained with the two considered sQN algorithms and the *tuned* Adam. We have analyzed which algorithm achieves the highest training accuracy within at most 10 epochs for different batch sizes. In networks with BN layers, all methods achieve comparable training and testing accuracy although sQN methods reach higher training accuracy than *tuned* Adam. We found that sL-BFGS-TR trains faster than both sL-SR1-TR and Adam for $bs = 100$ (see Figure 6 (b) and (d)). On the other hand, for networks without BN layers, sL-SR1-TR is the clear winner and sL-BFGS-TR performs very poorly in some cases. For instance, on the experiment to train ResNet-20(no BN) to classify Fashion-MNIST, sL-BFGS-TR exhibits worse performance (see Figure 6 (e)).

Another important observation is that the performance of Adam is more affected by batch sizes than that of sQN algorithms (see Figure 22 and 23, for instance), thus the advantage of sQN over Adam can increase in distributed implementations when using large batch sizes to enhance the parallel efficiency.

³Progressive batching strategies act naturally as a variance reduction technique.

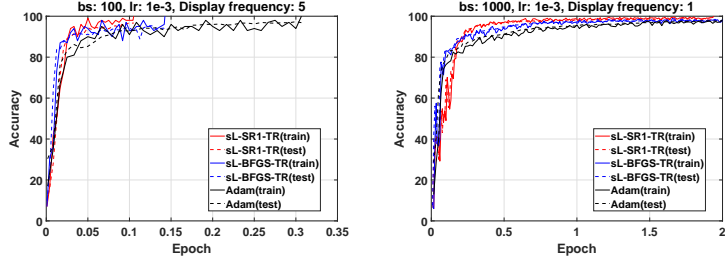


(a) *sL-BFGS-TR*

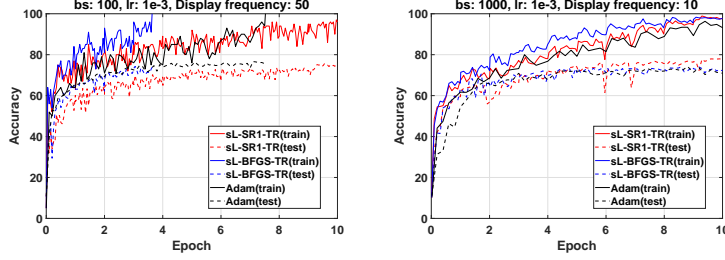


(b) *sL-SR1-TR*

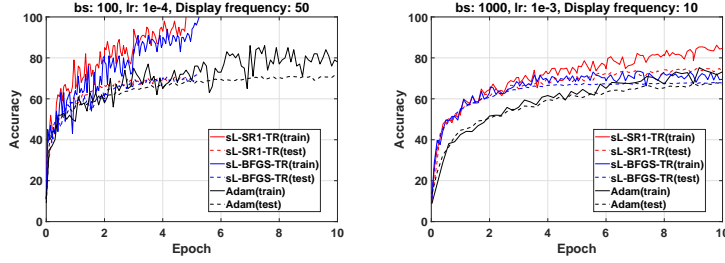
Figure 5 The performance of *sL-BFGS-TR* and *sL-SR1-TR* with different fixed batch sizes (*bs*) in comparison with the adaptive batching STORM algorithm [13, 5].



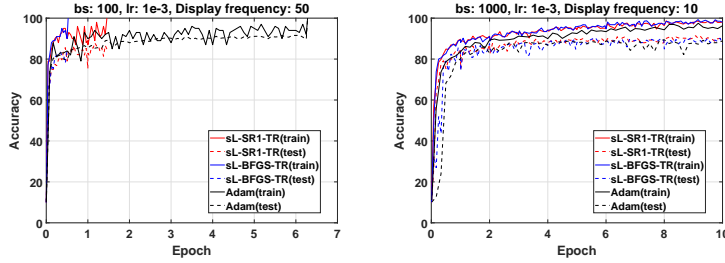
(a) MNIST with LeNet-like



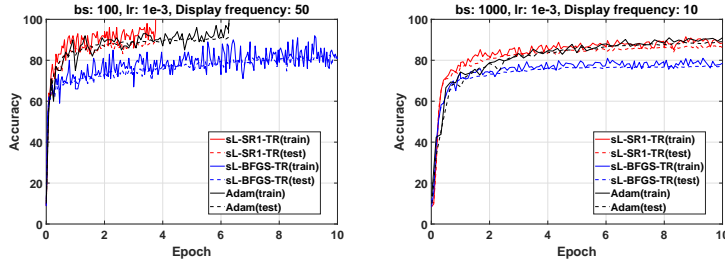
(b) CIFAR10 with ConvNet3FC2



(c) CIFAR10 with ConvNet3FC2(no BN)

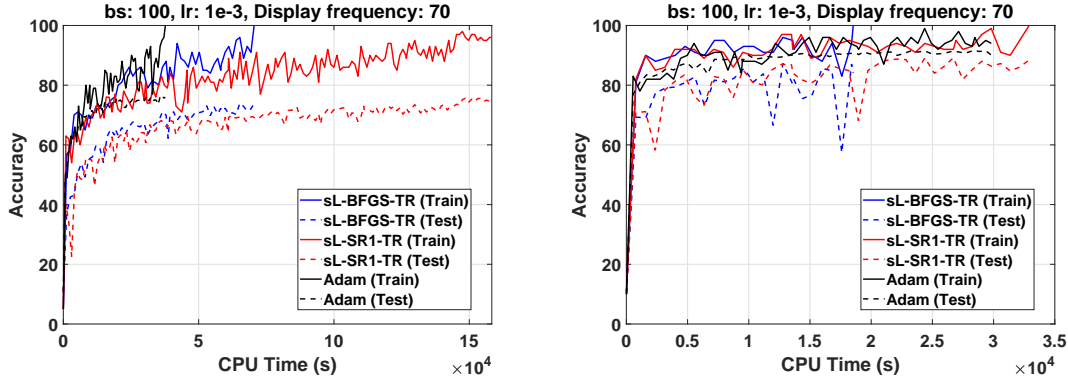


(d) Fashion-MNIST with ResNet-20



(e) Fashion-MNIST with ResNet-20(no BN)

Figure 6 Comparison of sL-BFGS-TR, sL-SR1-TR with $l = 20$ and tuned Adam with optimal learning rate (lr) for different batch sizes (bs).



(a) CIFAR10, ConvNet3FC2 (left), Fashion-MNIST, ResNet-20 (right)

Figure 7 Comparison in terms of CPU training time of sL-BFGS-TR, sL-SR1-TR with $l = 20$ and tuned Adam with optimal batch size (bs) and learning rate (lr).

7. Conclusions

We have studied stochastic QN methods for training deep neural networks. We have considered both L-SR1 and L-BFGS updates in a stochastic setting under a trust-region framework. An extensive experimental work including the effect of batch normalization (BN), the limited memory parameter, the sampling strategy and batch size has been reported and discussed. Our experiments show that BN is a key factor for the performance of stochastic QN algorithms, and that sL-SR1-TR performs better than sL-BFGS-TR in networks without BN layers. This behavior is in accordance with the property of L-SR1 updates allowing for indefinite Hessian approximations in non-convex optimization. However, sL-BFGS-TR behaves comparably or slightly better than sL-SR1-TR when BN layers are used.

Moreover, our experimental results have illustrated that employing larger batch sizes within a fixed number of epochs produces less training accuracy which can be recovered by longer training. Our experiments on training time have also shown a slight superiority in the accuracy reached by both algorithms when larger batch sizes are used within a fixed budget of time. This suggests the use of large batch sizes also in view of the parallelization of the algorithms. The proposed sQN algorithms, with overlapping fixed size sampling strategy, revealed more efficient than the STORM algorithm which relies on a progressive adaptive sampling strategy thus naturally incorporating a variance reduction technique. Finally, our results show that sQN methods in some instances outperform the well-known first-order Adam optimizer run with the optimal combination of its numerous parameters. We believe that this contribution fills a gap concerning the real performance of the SR1 and BFGS updates onto realistic large-size DNNs and is expected to help drive the researchers in this field to the choice of the proper quasi-Newton method.

References

- [1] L. Adhikari, O. DeGuchy, J.B. Erway, S. Lockhart, and R.F. Marcia, *Limited-memory trust-region methods for sparse relaxation*, in *Wavelets and Sparsity XVII*, Y.M. Lu, D. Van de Ville, and M. Papadakis, eds., Vol. 10394. International Society for Optics and Photonics, SPIE, 2017, pp. 95 – 102.

- [2] A.S. Berahas, M. Jahani, P. Richtárik, and M. Takáč, *Quasi-newton methods for deep learning: Forget the past, just sample*, Optimization Methods and Software (2021). Published online 15 Oct 2021.
- [3] A.S. Berahas, J. Nocedal, and M. Takáč, *A multi-batch L-BFGS method for machine learning*, Advances in Neural Information Processing Systems (2016), pp. 1063–1071.
- [4] A.S. Berahas and M. Takáč, *A robust multi-batch L-BFGS method for machine learning*, Optimization Methods and Software 35 (2020), pp. 191–219.
- [5] J. Blanchet, C. Cartis, M. Menickelly, and K. Scheinberg, *Convergence rate analysis of a stochastic trust-region method via supermartingales*, INFORMS journal on optimization 1 (2019), pp. 92–119.
- [6] R. Bollapragada, R.H. Byrd, and J. Nocedal, *Exact and inexact subsampled newton methods for optimization*, IMA Journal of Numerical Analysis 39 (2019), pp. 545–578.
- [7] R. Bollapragada, J. Nocedal, D. Mudigere, H.J. Shi, and P.T.P. Tang, *A progressive batching L-BFGS method for machine learning*, in *International Conference on Machine Learning*. PMLR, 2018, pp. 620–629.
- [8] L. Bottou, F.E. Curtis, and J. Nocedal, *Optimization methods for large-scale machine learning*, Siam Review 60 (2018), pp. 223–311.
- [9] L. Bottou and Y. LeCun, *Large scale online learning*, Advances in neural information processing systems 16 (2004), pp. 217–224.
- [10] J. Brust, J.B. Erway, and R.F. Marcia, *On solving L-SR1 trust-region subproblems*, Computational Optimization and Applications 66 (2017), pp. 245–266.
- [11] O. Burdakov, L. Gong, S. Zikrin, and Y.x. Yuan, *On efficiently combining limited-memory and trust-region techniques*, Mathematical Programming Computation 9 (2017), pp. 101–134.
- [12] R.H. Byrd, S.L. Hansen, J. Nocedal, and Y. Singer, *A stochastic quasi-newton method for large-scale optimization*, SIAM Journal on Optimization 26 (2016), pp. 1008–1031.
- [13] R. Chen, M. Menickelly, and K. Scheinberg, *Stochastic optimization using a trust-region method and random models*, Mathematical Programming 169 (2018), pp. 447–487.
- [14] A.R. Conn, N.I. Gould, and P.L. Toint, *Trust region methods*, SIAM, 2000.
- [15] A. Defazio, F. Bach, and S. Lacoste-Julien, *SAGA: A fast incremental gradient method with support for non-strongly convex composite objectives*, in *Advances in neural information processing systems*. 2014, pp. 1646–1654.
- [16] J. Duchi, E. Hazan, and Y. Singer, *Adaptive subgradient methods for online learning and stochastic optimization.*, Journal of machine learning research 12 (2011).
- [17] J.B. Erway, J. Griffin, R.F. Marcia, and R. Omheni, *Trust-region algorithms for training responses: machine learning methods using indefinite hessian approximations*, Optimization Methods and Software 35 (2020), pp. 460–487.

- [18] D.M. Gay, *Computing optimal locally constrained steps*, SIAM Journal on Scientific and Statistical Computing 2 (1981), pp. 186–197.
- [19] D. Goldfarb, Y. Ren, and A. Bahamou, *Practical quasi-newton methods for training deep neural networks*, Vol. 2020-December. 2020.
- [20] G. H. GOLUB AND C. F. VAN LOAN, *Matrix computations*, vol. 3, JHU press, 2013.
- [21] R. Gower, D. Goldfarb, and P. Richtárik, *Stochastic block BFGS: Squeezing more curvature out of data*, in *International Conference on Machine Learning*. PMLR, 2016, pp. 1869–1878.
- [22] K. He, X. Zhang, S. Ren, and J. Sun, *Deep residual learning for image recognition*, in *Proceedings of the IEEE conference on computer vision and pattern recognition*. 2016, pp. 770–778.
- [23] S. Ioffe, and C. Szegedy, *Batch normalization: Accelerating deep network training by reducing internal covariate shift*, in *International conference on machine learning*. PMLR, 2015, pp.448–456.
- [24] M. Jahani, M. Nazari, S. Rusakov, A.S. Berahas, and M. Takáč, *Scaling up quasi-newton algorithms: Communication efficient distributed SR1*, in *International Conference on Machine Learning, Optimization, and Data Science*. Springer, 2020, pp. 41–54.
- [25] R. Johnson and T. Zhang, *Accelerating stochastic gradient descent using predictive variance reduction*, Advances in neural information processing systems 26 (2013), pp. 315–323.
- [26] D.P. Kingma and J. Ba, *Adam: A method for stochastic optimization*, in *3rd International Conference on Learning Representations, ICLR 2015 - Conference Track Proceedings*. 2015.
- [27] A. Krizhevsky, G. Hinton, *et al.*, *Learning multiple layers of features from tiny images*, Available at: <https://www.cs.toronto.edu/~kriz/cifar.html> (2009).
- [28] S. Kylasa, F. Roosta, M.W. Mahoney, and A. Grama, *GPU accelerated sub-sampled Newton’s method for convex classification problems*, in *Proceedings of the 2019 SIAM International Conference on Data Mining*. SIAM, 2019, pp. 702–710.
- [29] Y. LeCun, *The mnist database of handwritten digits*, Available at: <http://yann.lecun.com/exdb/mnist/> (1998).
- [30] Y. LeCun, L. Bottou, Y. Bengio, and P. Haffner, *Gradient-based learning applied to document recognition*, Proceedings of the IEEE 86 (1998), pp. 2278–2324.
- [31] A. Lucchi, B. McWilliams, and T. Hofmann, *A variance reduced stochastic newton method*, arXiv preprint arXiv:1503.08316 (2015).
- [32] J. Martens and I. Sutskever, *Training deep and recurrent networks with hessian-free optimization*, in *Neural Networks: Tricks of the Trade*, Springer, 2012, pp. 479–535.

- [33] J. Martens, *et al.*, *Deep learning via hessian-free optimization.*, in *ICML*, Vol. 27. 2010, pp. 735–742.
- [34] A. Mokhtari and A. Ribeiro, *Res: Regularized stochastic BFGS algorithm*, *IEEE Transactions on Signal Processing* 62 (2014), pp. 6089–6104.
- [35] A. Mokhtari and A. Ribeiro, *Global convergence of online limited memory BFGS*, *The Journal of Machine Learning Research* 16 (2015), pp. 3151–3181.
- [36] J.J. Moré and D.C. Sorensen, *Computing a trust region step*, *SIAM Journal on Scientific and Statistical Computing* 4 (1983), pp. 553–572.
- [37] P. Moritz, R. Nishihara, and M. Jordan, *A linearly-convergent stochastic L-BFGS algorithm*, in *Artificial Intelligence and Statistics*. PMLR, 2016, pp. 249–258.
- [38] J. Nocedal and S. Wright, *Numerical optimization*, Springer Science & Business Media, 2006.
- [39] J. Rafati and R.F. Marcia, *Improving L-BFGS initialization for trust-region methods in deep learning*, in *2018 17th IEEE International Conference on Machine Learning and Applications (ICMLA)*. IEEE, 2018, pp. 501–508.
- [40] H. Robbins and S. Monro, *A stochastic approximation method*, *The annals of mathematical statistics* (1951), pp. 400–407.
- [41] M. Schmidt, N. Le Roux, and F. Bach, *Minimizing finite sums with the stochastic average gradient*, *Mathematical Programming* 162 (2017), pp. 83–112.
- [42] N.N. Schraudolph, J. Yu, and S. Günter, *A stochastic quasi-Newton method for online convex optimization*, in *Artificial intelligence and statistics*. PMLR, 2007, pp. 436–443.
- [43] T. Steihaug, *The conjugate gradient method and trust regions in large scale optimization*, *SIAM Journal on Numerical Analysis* 20 (1983), pp. 626–637.
- [44] X. Wang, S. Ma, D. Goldfarb, and W. Liu, *Stochastic quasi-newton methods for nonconvex stochastic optimization*, *SIAM Journal on Optimization* 27 (2017), pp. 927–956.
- [45] X. Wang and Y.x. Yuan, *Stochastic trust region methods with trust region radius depending on probabilistic models*, *arXiv preprint arXiv:1904.03342* (2019).
- [46] H. Xiao, K. Rasul, and R. Vollgraf, *Fashion-mnist: a novel image dataset for benchmarking machine learning algorithms*, *arXiv preprint arXiv:1708.07747* (2017).
- [47] P. Xu, F. Roosta, and M.W. Mahoney, *Second-order optimization for non-convex machine learning: An empirical study*, in *Proceedings of the 2020 SIAM International Conference on Data Mining*. SIAM, 2020, pp. 199–207.
- [48] L. Ziyin, B. Li, and M. Ueda, *SGD may never escape saddle points*, *arXiv preprint arXiv:2107.11774* (2021).
- [49] M. Yousefi, A. Martínez, *On the efficiency of Stochastic Quasi-Newton Methods for Deep Learning: supplementary material* (2022).

Appendix A. Solving the Trust-Region subproblem

Appendix A.1. Computing the search direction in the L-BFGS-TR method

We describe in this subsection how to solve the trust-region subproblem (7) where the BFGS Hessian approximation B_k is in compact form; see [1, 10, 39] for more details.

Let B_k be an L-BFGS compact matrix (3). Using Theorem 2.1, the global solution of the trust-region subproblem (7) can be obtained by exploiting the following two strategies:

Spectral decomposition of B_k . Computing the thin QR factorization of matrix Ψ_k , $\Psi_k = Q_k R_k$, or the Cholesky factorization of $\Psi_k^T \Psi_k$, $\Psi_k^T \Psi_k = R^T R$, and then spectrally decomposing the small matrix $R_k M_k R_k^T$ as $R_k M_k R_k^T = U_k \hat{\Lambda} U_k^T$ leads to

$$B_k = B_0 + Q_k R_k M_k R_k^T Q_k^T = \gamma_k I + Q_k U_k \hat{\Lambda} U_k^T Q_k^T,$$

where U_k and $\hat{\Lambda}$ are orthogonal and diagonal matrices, respectively. Let $P_{\parallel} \triangleq Q_k U_k$ (or $P_{\parallel} = (\Psi_k R_k^{-1} U_k)^T$) and $P_{\perp} \triangleq (Q_k U_k)^{\perp}$ where $(\cdot)^{\perp}$ denotes orthogonal complement. By Theorem 2.1.1 in [20], we have $P^T P = P P^T = I$ where

$$P \triangleq [P_{\parallel} \quad P_{\perp}] \in \mathbb{R}^{n \times n}. \quad (\text{A.1})$$

Therefore the spectral decomposition of B_k is obtained as

$$B_k = P \Lambda P^T, \quad \Lambda \triangleq \begin{bmatrix} \Lambda_1 & 0 \\ 0 & \Lambda_2 \end{bmatrix} = \begin{bmatrix} \hat{\Lambda} + \gamma_k I & 0 \\ 0 & \gamma_k I \end{bmatrix}, \quad (\text{A.2})$$

where Λ_1 consists of at most $2l$ eigenvalues as $\Lambda_1 = \text{diag}(\hat{\lambda}_1 + \gamma_k, \hat{\lambda}_2 + \gamma_k, \dots, \hat{\lambda}_{2l} + \gamma_k)$. We assume the eigenvalues are increasingly ordered.

Inversion by Sherman-Morrison-Woodbury formula. By dropping subscript k in (3) and using the Sherman-Morrison-Woodbury formula to compute the inverse of the coefficient matrix in (9), we have

$$p(\sigma) = -(B + \sigma I)^{-1} g = -\frac{1}{\tau} \left(I - \Psi (\tau M^{-1} + \Psi^T \Psi)^{-1} \Psi^T \right) g, \quad (\text{A.3})$$

where $\tau = \gamma + \sigma$. By using (A.2), the first optimality condition in (9) can be written as

$$(\Lambda + \sigma I) v = -P^T g, \quad (\text{A.4})$$

where

$$v = P^T p, \quad P^T g \triangleq \begin{bmatrix} g_{\parallel} \\ g_{\perp} \end{bmatrix} = \begin{bmatrix} P_{\parallel}^T g \\ P_{\perp}^T g \end{bmatrix}, \quad (\text{A.5})$$

and therefore

$$\|p(\sigma)\| = \|v(\sigma)\| = \sqrt{\left\{ \sum_{i=1}^k \frac{(g_{\parallel})_i^2}{(\lambda_i + \sigma)^2} \right\} + \frac{\|g_{\perp}\|^2}{(\gamma + \sigma)^2}}, \quad (\text{A.6})$$

where $\|g_{\perp}\|^2 = \|g\|^2 - \|g_{\parallel}\|^2$. This makes the computation of $\|p\|$ feasible without computing p explicitly. Let $p_u \triangleq p(0)$ as an unconstrained minimizer for (7) be the solution of the first optimality condition in (9), for which $\sigma = 0$ makes the second optimality condition hold. Now, we consider the following cases:

- If $\|p_u\| \leq \delta$, the optimal solution of (7) using (A.3) is computed as

$$(\sigma^*, p^*) = (0, p_u) = (0, p(0)). \quad (\text{A.7})$$

- If $\|p_u\| > \delta$, then p^* must lie on the boundary of the trust-region to hold the second optimality condition. To impose this, σ^* must be the root of the following equation which is determined by the Newton method proposed in [10]:

$$\phi(\sigma) \triangleq \frac{1}{\|p(\sigma)\|} - \frac{1}{\delta} = 0. \quad (\text{A.8})$$

Therefore, using (A.3), the global solution is computed as

$$(\sigma^*, p^*) = (\sigma^*, p(\sigma^*)). \quad (\text{A.9})$$

The procedure described in this section to solve the trust-region subproblem is illustrated in Algorithm 4 (see Appendix Appendix C).

Appendix A.2. Computing the search direction in the L-SR1-TR method

To solve (7) where B_k is a compact L-SR1 matrix (22), an efficient algorithm called the *Orthonormal Basis L-SR1* (OBS) was proposed in [10]. We summarize this approach here.

Let (A.2) be the eigenvalue decomposition of (22), where Λ_1 consists of at most r eigenvalues as $\Lambda_1 = \text{diag}(\hat{\lambda}_1 + \gamma_k, \hat{\lambda}_2 + \gamma_k, \dots, \hat{\lambda}_r + \gamma_k)$. We assume the eigenvalues are increasingly ordered. The OBS method exploits the Sherman-Morrison-Woodbury formula in different cases for L-SR1 B_k ; by dropping subscript k in (22), these cases are:

B is positive definite. In this case, the global solution of (7) is (A.7) or (A.9).

B is positive semi-definite (singular). Since $\gamma \neq 0$ and B is positive semi-definite with all non-negative eigenvalues, then $\lambda_{\min} = \min\{\lambda_1, \gamma\} = \lambda_1 = 0$. Let r be the multiplicity of the λ_{\min} ; therefore,

$$0 = \lambda_1 = \lambda_2 = \dots = \lambda_r < \lambda_{r+1} \leq \lambda_{r+2} \leq \dots \leq \lambda_k.$$

For $\sigma > -\lambda_{\min} = 0$, the matrix $(\Lambda + \sigma I)$ in (A.4) is invertible, and thus, $\|p(\sigma)\|$ in (A.6) is well-defined. For $\sigma = -\lambda_{\min} = 0$, we consider the two following sub-cases⁴:

1. If $\lim_{\sigma \rightarrow 0^+} \phi(\sigma) < 0$, then $\lim_{\sigma \rightarrow 0^+} \|p(\sigma)\| > \delta$. Here, the OBS algorithm uses Newton's method to find $\sigma^* \in (0, \infty)$ so that the global solution p^* lies on the boundary of trust-region, i.e., $\phi(\sigma^*) = 0$. This solution $p^* = p(\sigma^*)$ is computed using (A.3); by that, the global pair solution (σ^*, p^*) satisfies the first and second optimal conditions in (9).
2. If $\lim_{\sigma \rightarrow 0^+} \phi(\sigma) \geq 0$, then $\lim_{\sigma \rightarrow 0^+} \|p(\sigma)\| \leq \delta$. It can be proved that $\phi(\sigma)$ is strictly increasing for $\sigma > 0$ (see Lemma 7.3.1 in [14]). This makes $\phi(\sigma) \geq 0$ for $\sigma > 0$ as it is non-negative at 0^+ , and thus, $\phi(\sigma)$ can only have a root $\sigma^* = 0$ in $\sigma \geq 0$. Here, we should notice that even if $\phi(\sigma) > 0$, the solution $\sigma^* = 0$ makes the second optimality

⁴To have a well-defined expression in (A.6), we will discuss in limit setting (at $-\lambda_{\min}^+$).

condition in (9) hold. Since matrix $B + \sigma I$ at $\sigma^* = 0$ is not invertible, the global solution p^* for the first optimality condition in (9) is computed by

$$\begin{aligned} p^* &= p(\sigma^*) = -(B + \sigma^* I)^\dagger g = -P(\Lambda + \sigma^* I)^\dagger P^T g \\ &= -P_\parallel(\Lambda_1 + \sigma^* I)^\dagger P_\parallel^T g - \frac{1}{\gamma + \sigma^*} P_\perp P_\perp^T g \\ &= -\Psi R^{-1} U(\Lambda_1 + \sigma^* I)^\dagger g_\parallel - \frac{1}{\gamma + \sigma^*} P_\perp P_\perp^T g, \end{aligned} \quad (\text{A.10})$$

where $(g_\parallel)_i = (P_\parallel^T g)_i = 0$ for $i = 1, \dots, r$ if $\sigma^* = -\lambda_{\min} = -\lambda_1 = 0$, and

$$P_\perp P_\perp^T g = (I - P_\parallel P_\parallel^T)g = (I - \Psi R^{-1} R^{-T} \Psi^T)g.$$

Therefore, both optimality conditions in (9) hold for the pair solution (σ^*, p^*) .

B is indefinite. Let r be the algebraic multiplicity of the leftmost eigenvalue λ_{\min} . Since B is indefinite and $\gamma \neq 0$, we have $\lambda_{\min} = \min\{\lambda_1, \gamma\} < 0$.

Obviously, for $\sigma > -\lambda_{\min}$, the matrix $(\Lambda + \sigma I)$ in (A.4) is invertible, and thus, $\|p(\sigma)\|$ in (A.6) is well-defined. For $\sigma = -\lambda_{\min}$, we discuss the two following cases:

1. If $\lim_{\sigma \rightarrow -\lambda_{\min}^+} \phi(\sigma) < 0$, then $\lim_{\sigma \rightarrow -\lambda_{\min}^+} \|p(\sigma)\| > \delta$. The OBS algorithm uses Newton's method to find $\sigma^* \in (-\lambda_{\min}, \infty)$ as the root of $\phi(\sigma) = 0$ so that the global solution p^* lies on the boundary of trust-region. By using (A.3) to compute $p^* = p(\sigma^*)$, the pair (σ^*, p^*) satisfies the both conditions in (9).
2. If $\lim_{\sigma \rightarrow -\lambda_{\min}^+} \phi(\sigma) \geq 0$, then $\lim_{\sigma \rightarrow -\lambda_{\min}^+} \|p(\sigma)\| \geq \delta$. For $\sigma > -\lambda_{\min}$, we have $\phi(\sigma) \geq 0$ but the solution $\sigma^* = -\lambda_{\min}$ as the only root of $\phi(\sigma) = 0$ is a positive number, which cannot satisfy the second optimal condition when $\phi(\sigma)$ is strictly positive. Hence, we should consider the cases of equality and inequality separately:

Equality. Let $\lim_{\sigma \rightarrow -\lambda_{\min}^+} \phi(\sigma) = 0$. Since matrix $B + \sigma I$ at $\sigma^* = -\lambda_{\min}$ is not invertible, the global solution p^* for the first optimality condition in (9) is computed using (A.10) by

$$p^* = \begin{cases} -\Psi R^{-1} U(\Lambda_1 + \sigma^* I)^\dagger g_\parallel - \frac{1}{\gamma + \sigma^*} P_\perp P_\perp^T g, & \sigma^* \neq -\gamma, \\ -\Psi R^{-1} U(\Lambda_1 + \sigma^* I)^\dagger g_\parallel, & \sigma^* = -\gamma, \end{cases} \quad (\text{A.11})$$

where $g_\perp = P_\perp^T g = 0$, and thus $\|g_\perp\| = 0$ if $\sigma^* = -\lambda_{\min} = -\gamma$. Moreover, $(g_\parallel)_i = (P_\parallel^T g)_i = 0$ for $i = 1, \dots, r$ if $\sigma^* = -\lambda_{\min} = -\lambda_1$.

We note that both optimality conditions in (9) hold for the computed (σ^*, p^*) .

Inequality. Let $\lim_{\sigma \rightarrow -\lambda_{\min}^+} \phi(\sigma) > 0$, then $\lim_{\sigma \rightarrow -\lambda_{\min}^+} \|p(\sigma)\| < \delta$. As mentioned before, $\sigma = -\lambda_{\min} > 0$ cannot satisfy the second optimality condition. In this case, so-called *hard case*, we attempt to find a solution which lies on the boundary. For $\sigma^* = -\lambda_{\min}$, this optimal solution is given by

$$p^* = \hat{p}^* + z^*, \quad (\text{A.12})$$

where $\hat{p}^* = -(B + \sigma^* I)^\dagger g$ is computed by (A.11) and $z^* = \alpha u_{min}$. Vector u_{min} is a unit eigenvector in the subspace associated with λ_{min} and α is obtained so that $\|\hat{p}^*\| = \delta$; i.e.,

$$\alpha = \sqrt{\delta^2 - \|\hat{p}^*\|^2}. \quad (\text{A.13})$$

The computation of u_{min} depends on $\lambda_{min} = \min\{\lambda_1, \gamma\}$. If $\lambda_{min} = \lambda_1$ then the first column of P is a leftmost eigenvector of B , and thus, u_{min} is set to the first column of P_{\parallel} . On other hand, if $\lambda_{min} = \gamma$, then any vector in the column space of P_{\perp} will be an eigenvector of B corresponding to λ_{min} . However, we avoid forming matrix P_{\perp} to compute $P_{\perp} P_{\perp}^T g$ in (A.11) if $\lambda_{min} = \lambda_1$. By the definition (A.1), we have

$$\text{Range}(P_{\perp}) = \text{Range}(P_{\parallel})^{\perp}, \quad \text{Range}(P_{\parallel}) = \text{Ker}(I - P_{\parallel} P_{\parallel}^T).$$

To find a vector in the column space of P_{\perp} , we use $I - P_{\parallel} P_{\parallel}^T$ as projection matrix mapping onto the column space of P_{\perp} . For simplicity, we can map one canonical basis vector at a time onto the column space of P_{\perp} until a nonzero vector is obtained. This practical process, repeated at most $k + 1$ times, will result in a vector that lies in $\text{Range}(P_{\perp})$; i.e.,

$$u_{min} \triangleq (I - P_{\parallel} P_{\parallel}^T) e_j, \quad (\text{A.14})$$

for $j = 1, 2, \dots, k + 1$ with $\|u_{min}\| \neq 0$; because $e_j \in \text{Range}(P_{\parallel})$ and

$$\text{rank}(P_{\parallel}) = \dim \text{Range}(P_{\parallel}) = \dim \text{Ker}(I - P_{\parallel} P_{\parallel}^T) = k.$$

Algorithm 5 (see [Appendix Appendix C](#)) describes how to solve the TR subproblem for the optimal search direction p^* .

Appendix B. Extended numerical results

Further figures of numerical results on different classification problems listed in [Table 3](#) are provided in the supplementary material [49].

Appendix C. Algorithms

In this section, all algorithms considered in this work are described in detail along with the values of the hyper-parameters used in the experiments.

Algorithm 3 Overlapping multi-batch generation

- 1: **Inputs:** os , N , \bar{N} , shuffled dataset and current iteration k
 - 2: **if** $\text{mod}(k + 1, \bar{N}) \neq 0$ **then**
 - 3: Create two subsets O_{k-1} and O_k of size os
 - 4: **else**
 - 5: **if** $\text{mod}(N, os) = 0$ **then**
 - 6: Create two subsets O_{k-1} and O_k of size os for last multi-batch J_k
 - 7: **else**
 - 8: Create three subsets O_{k-1} , O_k of size os and R_k of size $\text{mod}(N, os) = 0$ for last multi-batch J_k
 - 9: **end if**
 - 10: Shuffle data without replacement for the next epoch
 - 11: **end if**
-

Algorithm 4 Orthonormal basis BFGS

- 1: **Inputs:** Current iteration k , $\delta \triangleq \delta_k$, $g \triangleq g_k$ and $B \triangleq B_k : \Psi \triangleq \Psi_k, M^{-1} \triangleq M_k^{-1}, \gamma \triangleq \gamma_k$
 - 2: Compute the thin QR factors Q and R of Ψ or the Cholesky factor R of $\Psi^T \Psi$
 - 3: Compute the spectral decomposition of matrix $RM R^T = U \hat{\Lambda} U^T$
 - 4: Set $\hat{\Lambda} = \text{diag}(\hat{\lambda}_1, \dots, \hat{\lambda}_k)$ such that $\hat{\lambda}_1 \leq \dots \leq \hat{\lambda}_k$ and $\lambda_{\min} = \min\{\lambda_1, \gamma\}$ with algebraic multiplicity r
 - 5: Compute the spectral of B_k as $\Lambda_1 = \hat{\Lambda} + \gamma I$
 - 6: Compute $P_{\parallel} = QU$ or $P_{\parallel} = (\Psi R^{-1} U)^T$ and $g_{\parallel} = P_{\parallel}^T g$
 - 7: **if** $\phi(0) \geq 0$ **then**
 - 8: Set: $\sigma^* = 0$
 - 9: Compute p^* with (A.3) as solution of $(B_k + \sigma^* I)p = -g$
 - 10: **else**
 - 11: Compute a root $\sigma^* \in (0, \infty)$ of (A.8) by Newton method [10]
 - 12: Compute p^* with (A.3) as solution of $(B_k + \sigma^* I)p = -g$
 - 13: **end if**
-

Algorithm 5 Orthonormal Basis SR1 (OBS)

- 1: **Inputs:** Current iteration k , $\delta \triangleq \delta_k$, $g \triangleq g_k$ and $B \triangleq B_k : \Psi \triangleq \Psi_k, M^{-1} \triangleq M_k^{-1}, \gamma \triangleq \gamma_k$
 - 2: Compute the thin QR factors Q and R of Ψ or the Cholesky factor R of $\Psi^T \Psi$
 - 3: Compute the spectral decomposition of matrix $RM R^T = U \hat{\Lambda} U^T$
 - 4: Set $\hat{\Lambda} = \text{diag}(\hat{\lambda}_1, \dots, \hat{\lambda}_k)$ such that $\hat{\lambda}_1 \leq \dots \leq \hat{\lambda}_k$ and $\lambda_{\min} = \min\{\lambda_1, \gamma\}$ with algebraic multiplicity r
 - 5: Compute the spectral of B_k as $\Lambda_1 = \hat{\Lambda} + \gamma I$
 - 6: Compute $P_{\parallel} = QU$ or $P_{\parallel} = (\Psi R^{-1} U)^T$ and $g_{\parallel} = P_{\parallel}^T g$
 - 7: {feasible constraint: $\phi(-\lambda_{\min}) \geq 0$ }
 - 8: **if** Case I: $\lambda_{\min} > 0$ and $\phi(0) \geq 0$ **then**
 - 9: Set: $\sigma^* = 0$
 - 10: Compute p^* with (A.3) as solution of $(B_k + \sigma^* I)p = -g$
 - 11: **else if** Case II: $\lambda_{\min} \leq 0$ and $\phi(-\lambda_{\min}) \geq 0$ **then**
 - 12: Set: $\sigma^* = -\lambda_{\min}$
 - 13: Compute p^* with (A.10) as solution of $(B_k + \sigma^* I)p = -g$
 - 14: **if** Case III: $\lambda_{\min} < 0$ **then**
 - 15: Compute α and u_{\min} with (A.12) for $z^* = \alpha u_{\min}$
 - 16: Update: $p^* = p^* + z^*$
 - 17: **end if**
 - 18: {infeasible constraint: $\phi(-\lambda_{\min}) < 0$ }
 - 19: **else**
 - 20: Compute a root $\sigma^* \in (\max\{-\lambda_{\min}, 0\}, \infty)$ of (A.8) by Newton method [10]
 - 21: Compute p^* with (A.3) as solution of $(B_k + \sigma^* I)p = -g$
 - 22: **end if**
-

Algorithm 6 Trust-region radius adjustment

- 1: **Inputs:** Current iteration k , $\delta_k, \rho_k, 0 < \tau_2 < 0.5 < \tau_3 < 1, 0 < \eta_2 \leq 0.5, 0.5 < \eta_3 < 1 < \eta_4$ ⁵
 - 2: **if** $\rho_k > \tau_3$ **then**
 - 3: **if** $\|p_k\| \leq \eta_3 \delta_k$ **then**
 - 4: $\delta_{k+1} = \delta_k$
 - 5: **else**
 - 6: $\delta_{k+1} = \eta_4 \delta_k$
 - 7: **end if**
 - 8: **else if** $\tau_2 \leq \rho_k \leq \tau_3$ **then**
 - 9: $\delta_{k+1} = \delta_k$
 - 10: **else**
 - 11: $\delta_{k+1} = \eta_2 \delta_k$
 - 12: **end if**
-

Algorithm 7 L-BFGS-TR

```
1: Inputs:  $w_0 \in \mathbb{R}^n$ ,  $\epsilon > 0$ ,  $\text{epoch}_{max}$ ,  $l$ ,  $\gamma_0 > 0$ ,  $S_0 = Y_0 = []$ ,  $\delta_0 > 0$ ,  $0 < \tau_1, \tau < 1$  a
2: Compute  $f_0$  and  $g_0$  by (2)
3: for  $k = 0, 1, \dots$  do
4:   if  $\text{mod}(k+1, \bar{N}) = 0$  then
5:     Shuffle the data without replacement for the next epoch and  $\text{epoch} = \text{epoch} + 1$ 
6:   end if
7:   {Check exit condition}
8:   if  $\|g_k\| \leq \epsilon$  or  $\text{epoch} > \text{epoch}_{max}$  then
9:     Stop training
10:  end if
11:  {Compute  $p \triangleq p_k^*$ }
12:  if  $k = 0$  then
13:    Compute  $p = -\delta_k \frac{g_k}{\|g_k\|}$ 
14:  else
15:    Compute  $p$  using Algorithm 4
16:  end if
17:  {Compute trial  $w_t$ }
18:  Compute  $w_t = w_k + p$  and then  $f_t$  and  $g_t$  by (2)
19:  {Curvature pair and  $\rho_k$ }
20:  Compute  $(s_k, y_k) = (w_t - w_k, g_t - g_k)$  and  $\rho_k = \frac{f_t - f_k}{Q(p)}$ 
21:  {Update  $w_k$ }
22:  if  $\rho_k \geq \tau_1$  then
23:     $w_{k+1} = w_t$ 
24:  else
25:     $w_{k+1} = w_k$ 
26:  end if
27:  {Update  $\delta_k$ }
28:  Update  $\delta_k$  by Algorithm 6
29:  {Update  $B_k$ }
30:  if  $s_k^T y_k > \tau \|s_k\|^2$  then
31:    if  $k < l$  then
32:      Store  $s_k$  and  $y_k$  as new columns in  $S_{k+1}$  and  $Y_{k+1}$ 
33:    else
34:      Keep only  $l$  most recent  $\{s_j, y_j\}_{j=k-l+1}^k$  in  $S_{k+1}$  and  $Y_{k+1}$ 
35:    end if
36:    Compute  $\gamma_{k+1}$  for  $B_0$  by Algorithm 8 and  $\Psi_{k+1}$ ,  $M_{k+1}^{-1}$  by (3)
37:  else
38:    Set  $\gamma_{k+1} = \gamma_k$ ,  $\Psi_{k+1} = \Psi_k$  and  $M_{k+1}^{-1} = M_k^{-1}$ 
39:  end if
40: end for
```

^a $\epsilon = 10^{-5}$, $\text{epoch}_{max} = 10$, $\gamma_0 = 1$, $\delta_0 = 1$, $\tau_1 = 10^{-4}$, $\tau = 10^{-2}$

Algorithm 8 L-BFGS Hessian initialization

```
1: Inputs: Current iteration  $k$  and storage matrices  $S_{k+1}$ ,  $Y_{k+1}$ ,  $c = 0.9$ .
2: Compute the smallest eigenvalue  $\hat{\lambda}$  of (19)
3: if  $\hat{\lambda} > 0$  then
4:    $\gamma_{k+1} = \max\{1, c\hat{\lambda}\} \in (0, \hat{\lambda})$ 
5: else
6:   Compute  $\gamma_k^h$  by (16) and set  $\gamma_{k+1} = \max\{1, \gamma_k^h\}$ 
7: end if
```

Algorithm 9 L-SR1-TR

```

1: Inputs:  $w_0 \in \mathbb{R}^n$ ,  $\epsilon > 0$ ,  $\text{epoch}_{max}$ ,  $l$ ,  $\gamma_0 > 0$ ,  $S_0 = Y_0 = []$ ,  $\delta_0 > 0$ ,  $0 < \tau_1, \tau < 1$  a
2: Compute  $f_0$  and  $g_0$  by (2)
3: for  $k = 0, 1, \dots$  do
4:   if  $\text{mod}(k+1, \bar{N}) = 0$  then
5:     Shuffle the data without replacement for the next epoch and  $\text{epoch} = \text{epoch} + 1$ 
6:   end if
7:   {Check exit condition}
8:   if  $\|g_k\| \leq \epsilon$  or  $\text{epoch} > \text{epoch}_{max}$  then
9:     Stop training
10:  end if
11:  {Compute  $p \triangleq p_k^*$ }
12:  if  $k = 0$  then
13:    Compute  $p = -\delta_k \frac{g_k}{\|g_k\|}$ 
14:  else
15:    Compute  $p$  using Algorithm 5
16:  end if
17:  {Compute trial  $w_t$ }
18:  Compute  $w_t = w_k + p$  and then  $f_t$  and  $g_t$  by (2)
19:  {Curvature pair and  $\rho_k$ }
20:  Compute  $(s_k, y_k) = (w_t - w_k, g_t - g_k)$  and  $\rho_k = \frac{f_t - f_k}{Q(p)}$ 
21:  {Update  $w_k$ }
22:  if  $\rho_k \geq \tau_1$  then
23:     $w_{k+1} = w_t$ 
24:  else
25:     $w_{k+1} = w_k$ 
26:  end if
27:  {Update  $\delta_k$ }
28:  Update:  $\delta_k$  with Algorithm 6
29:  {Update  $B_k$ }
30:  if  $|s^T(y_k - B_k s_k)| \geq \tau \|s_k\| \|y_k - B_k s_k\|$  then
31:    if  $k < l$  then
32:      Store  $s_k$  and  $y_k$  as new columns in  $S_{k+1}$  and  $Y_{k+1}$ 
33:    else
34:      Keep only  $l$  most recent  $\{s_j, y_j\}_{j=k-l+1}^k$  in  $S_{k+1}$  and  $Y_{k+1}$ 
35:    end if
36:    Compute  $\gamma_{k+1}$  for  $B_0$  by Algorithm 10 and  $\Psi_{k+1}, M_{k+1}^{-1}$  by (23)
37:  else
38:    Set  $\gamma_{k+1} = \gamma_k$ ,  $\Psi_{k+1} = \Psi_k$  and  $M_{k+1}^{-1} = M_k^{-1}$ 
39:  end if
40: end for

```

^a $\epsilon = 10^{-5}$, $\text{epoch}_{max} = 10$, $\gamma_0 = 1$, $\delta_0 = 1$, $\tau_1 = 10^{-4}$, $\tau = 10^{-8}$

Algorithm 10 L-SR1 Hessian initialization

```

1: Inputs: Current iteration  $k$  and storage matrices  $S_{k+1}, Y_{k+1}$  a
2: Compute the smallest eigenvalue  $\hat{\lambda}$  of (19)
3: if  $\hat{\lambda} > 0$  then
4:    $\gamma_{k+1} = \max\{c, c_1 \hat{\lambda}\}$ 
5: else
6:    $\gamma_{k+1} = \min\{-c, c_2 \hat{\lambda}\}$ 
7: end if

```

^a $c_1 = 0.5$, $c_2 = 1.5$, $c = 10^{-6}$

Algorithm 11 sL-BFGS-TR

```

1: Inputs:
   •  $w_0 \in \mathbb{R}^n$ ,  $\epsilon > 0$ ,  $\text{epoch}_{max}$ ,  $l$ ,  $\gamma_0 > 0$ ,  $S_0 = Y_0 = [\ ]$ ,  $\delta_0 > 0$ ,  $0 < \tau_1, \tau < 1$  a
2: while True do
3:   if  $k = 0$  then
4:     Take first and second subsets  $O_{-1}$  and  $O_0$  of size  $os$  for the initial multi-batch  $J_0$ 
5:     Compute  $f_0^{O_{-1}}$ ,  $g_0^{O_{-1}}$  and  $f_0^{O_0}$ ,  $g_0^{O_0}$  by (24) and then  $f_0^{J_0}$ ,  $g_0^{J_0}$  by (28)
6:   else
7:     Take the second subset  $O_k$  of size  $os$  for the multi-batch  $J_k$ 
8:     Compute  $f_k^{O_k}$ ,  $g_k^{O_k}$  by (24), and then  $f_k^{J_k}$ ,  $g_k^{J_k}$  by (28)
9:     if  $\text{mod}(k+1, \bar{N}) = 0$  then
10:      Shuffle the data without replacement for the next epoch and  $\text{epoch} = \text{epoch} + 1$ 
11:    end if
12:  end if
13:  {Check exit condition}
14:  if  $\|g_k^{J_k}\| \leq \epsilon$  or  $\text{epoch} > \text{epoch}_{max}$  then
15:    Stop training
16:  end if
17:  {Compute search direction}
18:  if  $k = 0$  then
19:    Compute  $p_k = -\delta_k \frac{g_k^{J_k}}{\|g_k^{J_k}\|}$ 
20:  else
21:    Compute  $p_k$  using Algorithm 4
22:  end if
23:  {Compute trial  $w_t$ }
24:  Compute  $w_t = w_k + p_k$ 
25:  Compute  $f_t^{O_{k-1}}$ ,  $g_t^{O_{k-1}}$  and  $f_t^{O_k}$ ,  $g_t^{O_k}$  by (24) and then  $f_t^{J_k}$ ,  $g_t^{J_k}$  by (28)
26:  {Compute curvature pair and  $\rho_k$ }
27:  Compute  $(s_k, y_k) = (w_t - w_k, g_t^{J_k} - g_k^{J_k})$  and  $\rho_k = \frac{f_t^{J_k} - f_k^{J_k}}{Q(p_k)}$ 
28:  if  $\rho_k \geq \tau_1$  then
29:     $w_{k+1} = w_t$  {Update  $w_k$ }
30:  else
31:     $w_{k+1} = w_k$ 
32:  end if
33:  Update  $\delta_k$  by Algorithm 6 {Update  $\delta_k$ }
34:  if  $s_k^T y_k > \tau \|s_k\|^2$  then
35:    if  $k < l$  then
36:      Store  $s_k$  and  $y_k$  as new columns in  $S_{k+1}$  and  $Y_{k+1}$  {Update  $B_k$ }
37:    else
38:      Keep only  $l$  recent  $\{s_j, y_j\}_{j=k-l+1}^k$  in  $S_{k+1}$  and  $Y_{k+1}$ 
39:    end if
40:    Compute  $\gamma_{k+1}$  for  $B_0$  by Algorithm 8 and  $\Psi_{k+1}$ ,  $M_{k+1}^{-1}$  by (3)
41:  else
42:    Set  $\gamma_{k+1} = \gamma_k$ ,  $\Psi_{k+1} = \Psi_k$  and  $M_{k+1}^{-1} = M_k^{-1}$ 
43:  end if
44:   $k = k + 1$ 
45: end while

```

^a $\epsilon = 10^{-5}$, $\text{epoch}_{max} = 10$, $\gamma_0 = 1$, $\delta_0 = 1$, $\tau_1 = 10^{-4}$, $\tau = 10^{-2}$

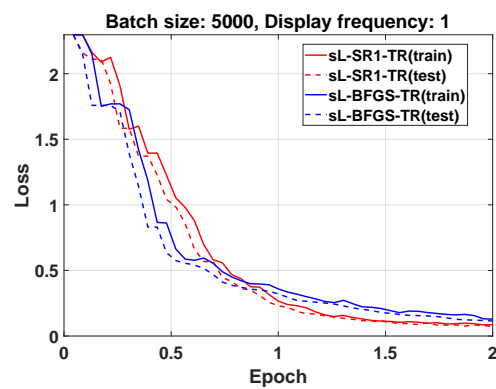
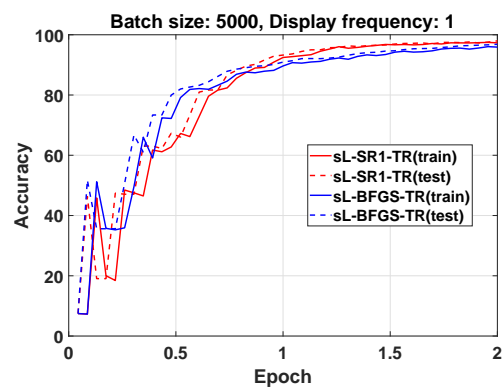
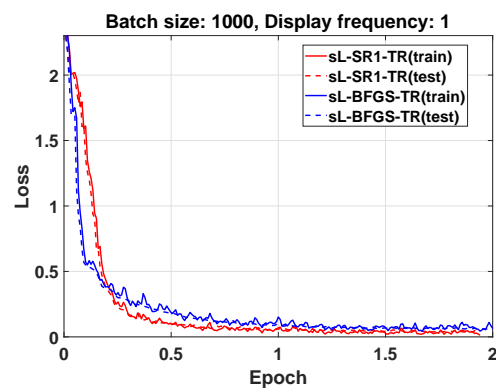
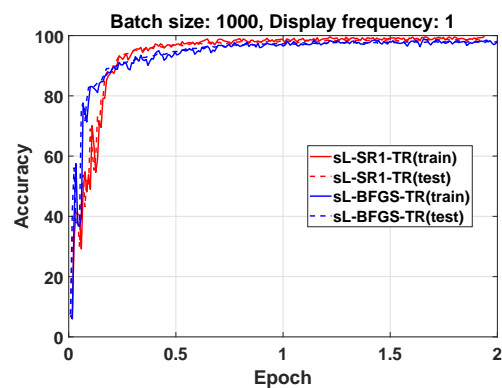
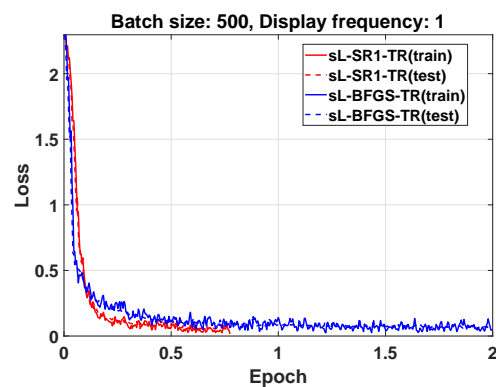
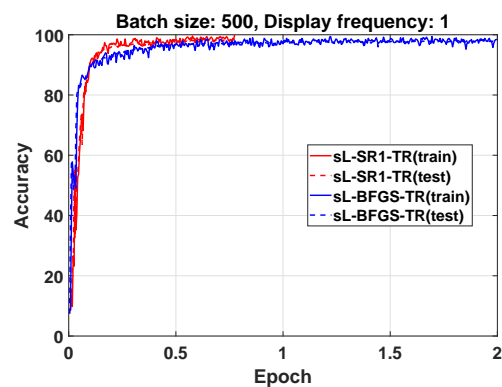
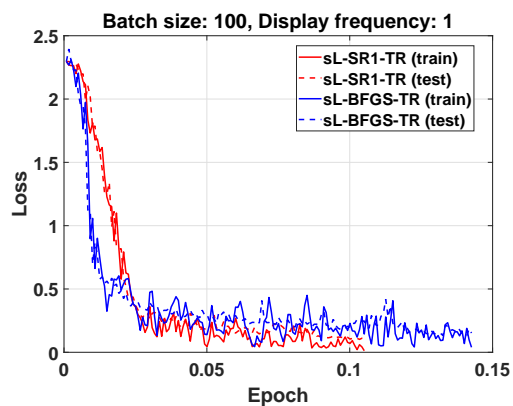
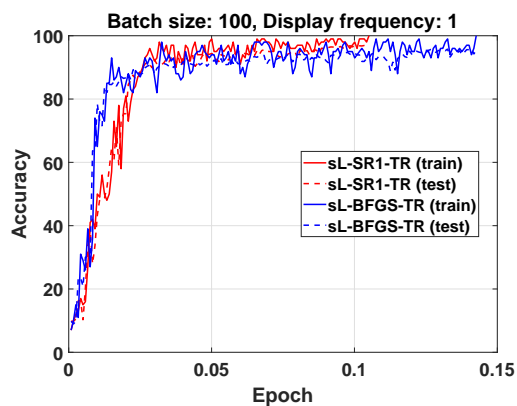
Algorithm 12 sL-SR1-TR

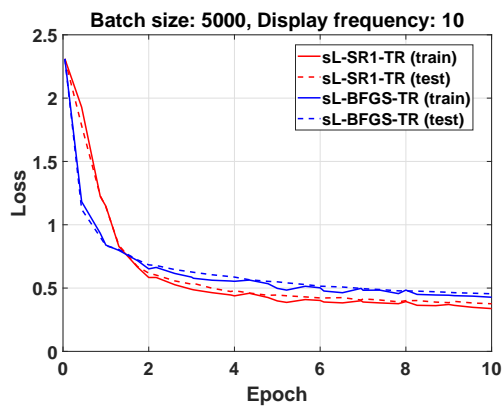
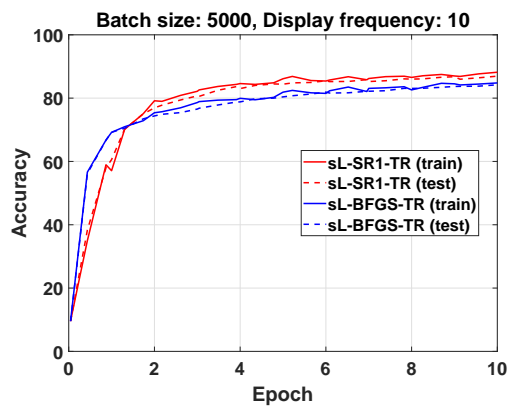
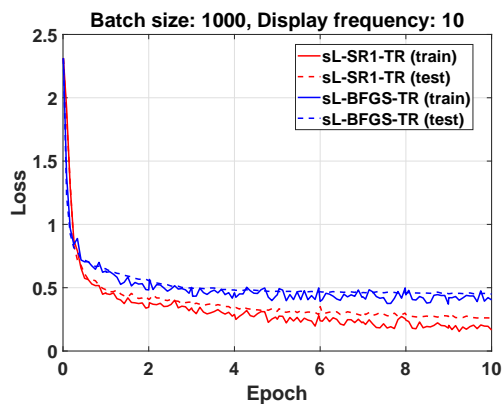
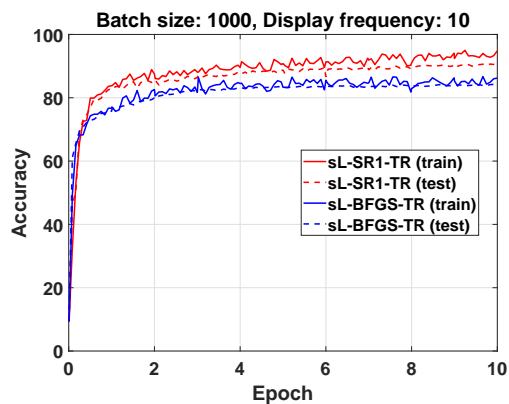
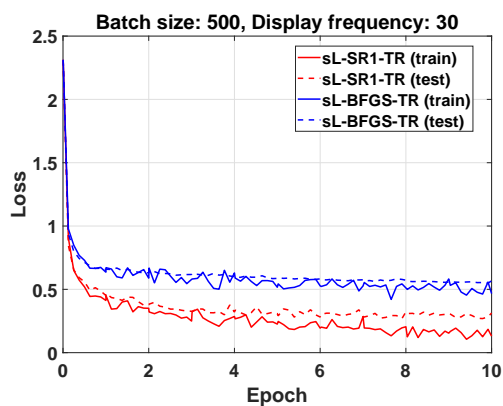
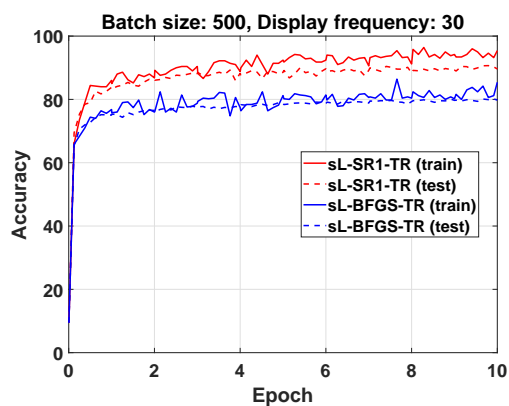
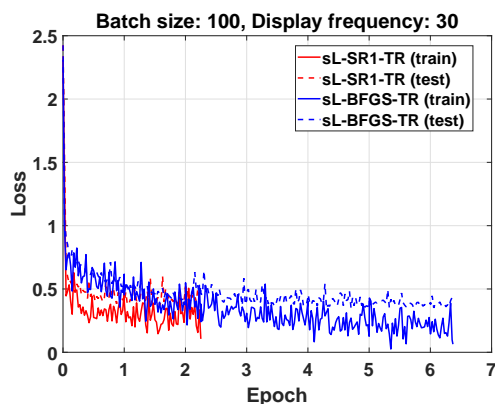
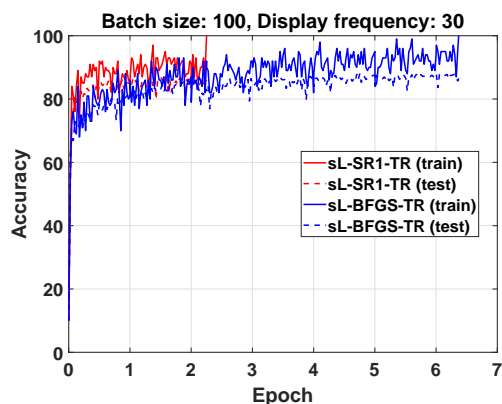
```

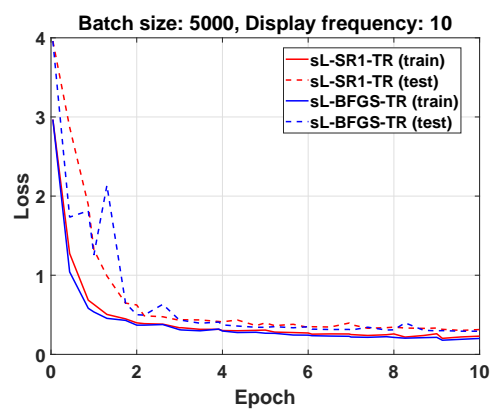
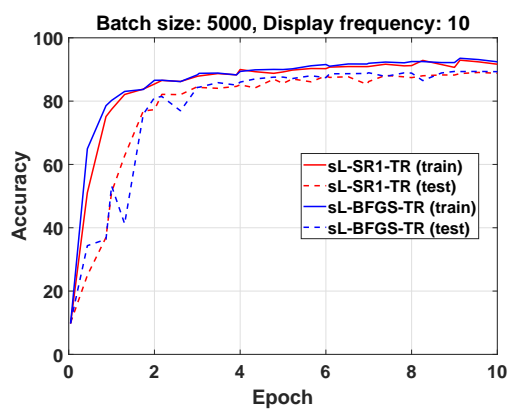
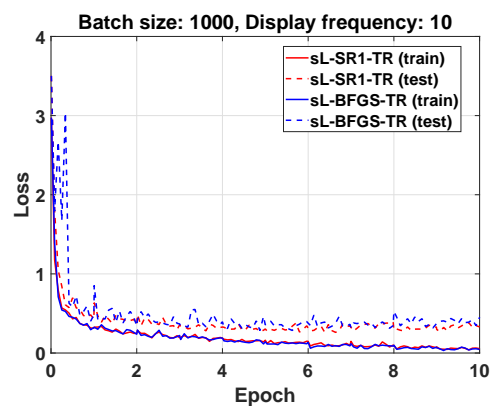
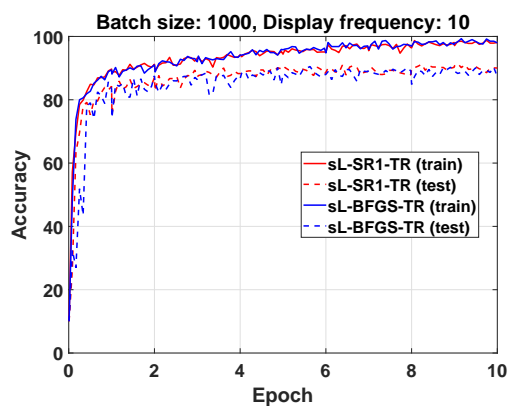
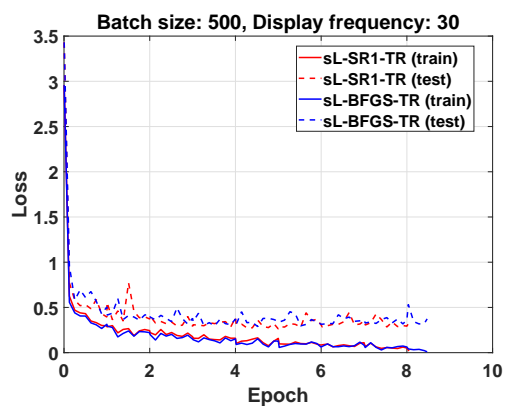
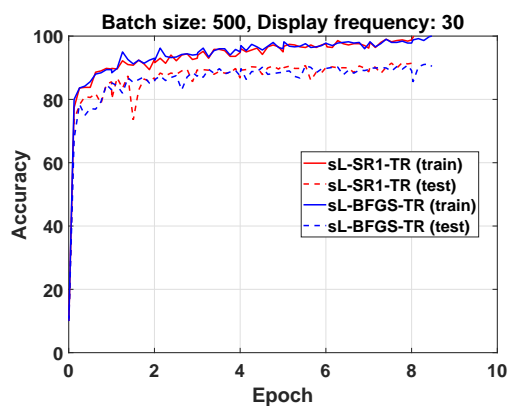
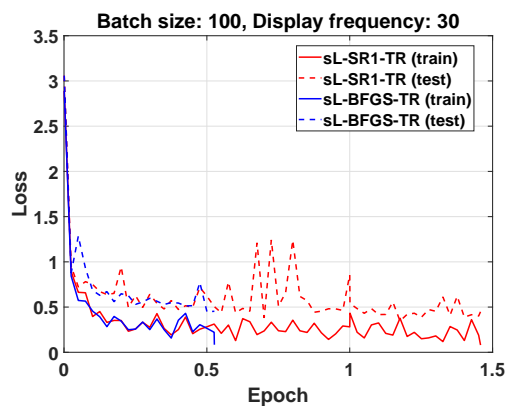
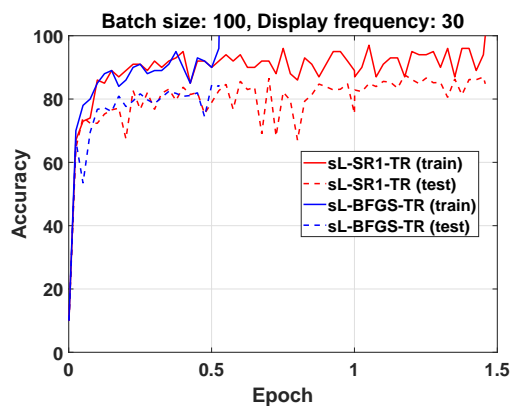
1: Inputs:
   •  $w_0 \in \mathbb{R}^n$ ,  $\epsilon > 0$ ,  $\text{epoch}_{max}$ ,  $l$ ,  $\gamma_0 > 0$ ,  $S_0 = Y_0 = [\ ]$ ,  $\delta_0 > 0$ ,  $0 < \tau_1, \tau < 1$  a
2: while True do
3:   if  $k = 0$  then
4:     Take first and second subsets  $O_{-1}$  and  $O_0$  of size  $os$  for the initial multi-batch  $J_0$ 
5:     Compute  $f_0^{O_{-1}}$ ,  $g_0^{O_{-1}}$  and  $f_0^{O_0}$ ,  $g_0^{O_0}$  by (24) and then  $f_0^{J_0}$ ,  $g_0^{J_0}$  by (28)
6:   else
7:     Take the second subset  $O_k$  of size  $os$  for the multi-batch  $J_k$ 
8:     Compute  $f_k^{O_k}$ ,  $g_k^{O_k}$  by (24), and then  $f_k^{J_k}$ ,  $g_k^{J_k}$  by (28)
9:     if  $\text{mod}(k+1, \bar{N}) = 0$  then
10:      Shuffle the data without replacement for the next epoch and  $\text{epoch} = \text{epoch} + 1$ 
11:    end if
12:  end if
13:  {Check exit condition}
14:  if  $\|g_k^{J_k}\| \leq \epsilon$  or  $\text{epoch} > \text{epoch}_{max}$  then
15:    Stop training
16:  end if
17:  {Compute search direction}
18:  if  $k = 0$  then
19:    Compute  $p_k = -\delta_k \frac{g_k^{J_k}}{\|g_k^{J_k}\|}$ 
20:  else
21:    Compute  $p_k$  using Algorithm 4
22:  end if
23:  {Compute trial  $w_t$ }
24:  Compute  $w_t = w_k + p_k$ 
25:  Compute  $f_t^{O_{k-1}}$ ,  $g_t^{O_{k-1}}$  and  $f_t^{O_k}$ ,  $g_t^{O_k}$  by (24) and then  $f_t^{J_k}$ ,  $g_t^{J_k}$  by (28)
26:  {Compute curvature pair and  $\rho_k$ }
27:  Compute  $(s_k, y_k) = (w_t - w_k, g_t^{J_k} - g_k^{J_k})$  and  $\rho_k = \frac{f_t^{J_k} - f_k^{J_k}}{Q(p_k)}$ 
28:  if  $\rho_k \geq \tau_1$  then
29:     $w_{k+1} = w_t$  {Update  $w_k$ }
30:  else
31:     $w_{k+1} = w_k$ 
32:  end if
33:  Update  $\delta_k$  by Algorithm 6 {Update  $\delta_k$ }
34:  if  $|s^T(y_k - B_k s_k)| \geq \tau \|s_k\| \|y_k - B_k s_k\|$  then
35:    if  $k \leq l$  then
36:      Store  $s_k$  and  $y_k$  as new columns in  $S_{k+1}$  and  $Y_{k+1}$  {Update  $B_k$ }
37:    else
38:      Keep only  $l$  recent  $\{s_j, y_j\}_{j=k-l+1}^k$  in  $S_{k+1}$  and  $Y_{k+1}$ 
39:    end if
40:    Compute  $\gamma_{k+1}$  for  $B_0$  by Algorithm 10 and  $\Psi_{k+1}$ ,  $M_{k+1}^{-1}$  by (23)
41:  else
42:    Set  $\gamma_{k+1} = \gamma_k$ ,  $\Psi_{k+1} = \Psi_k$  and  $M_{k+1}^{-1} = M_k^{-1}$ 
43:  end if
44:   $k = k + 1$ 
45: end while

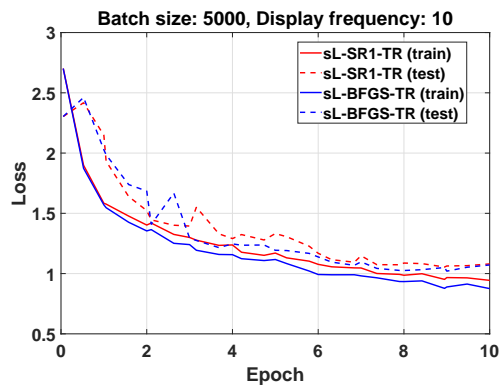
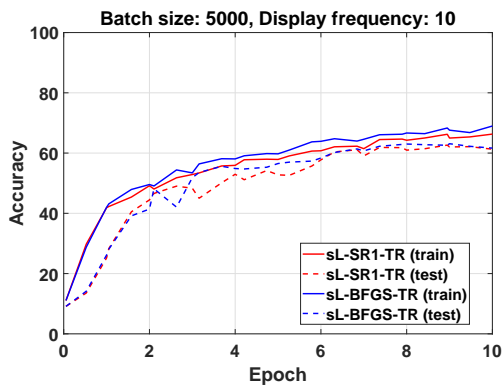
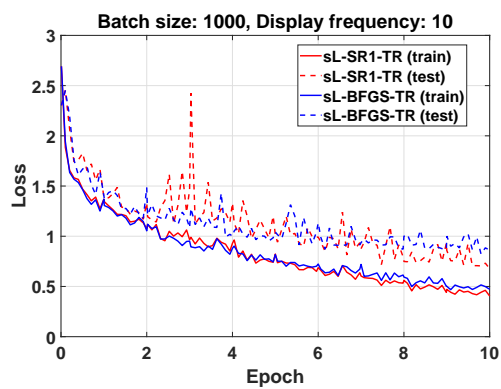
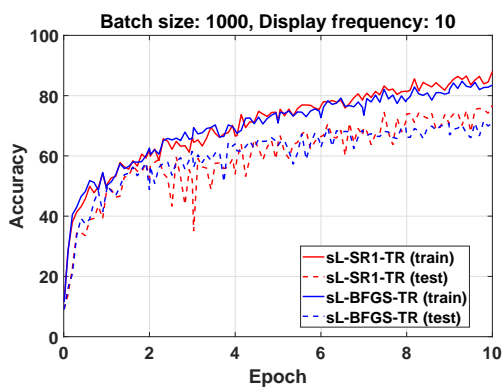
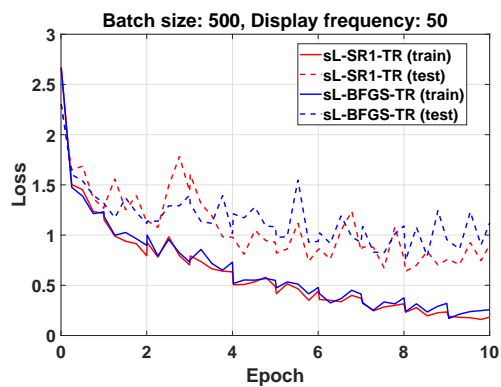
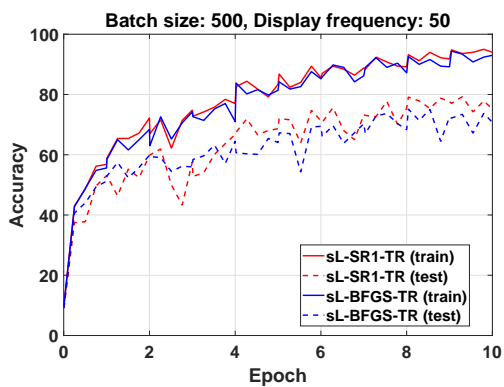
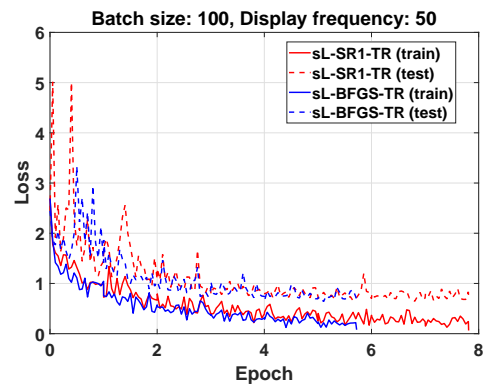
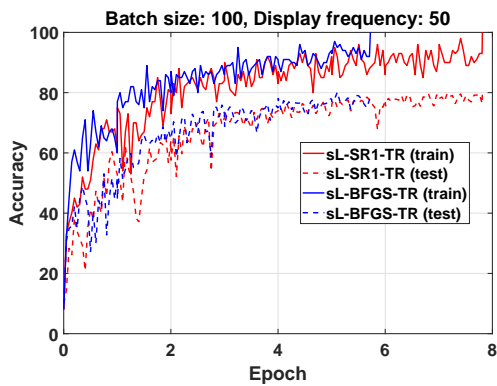
```

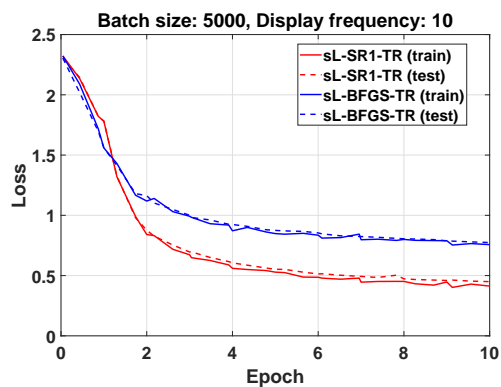
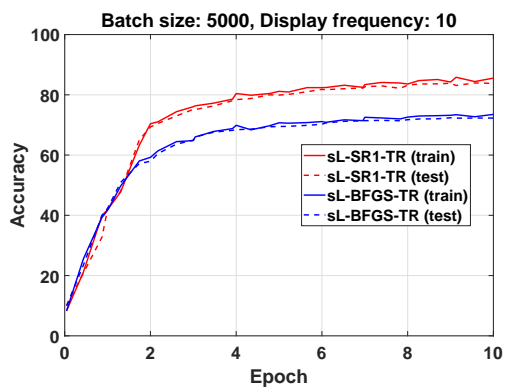
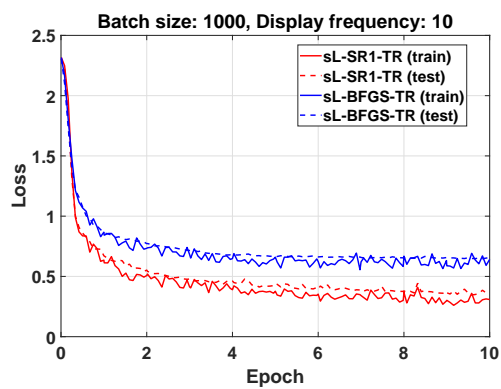
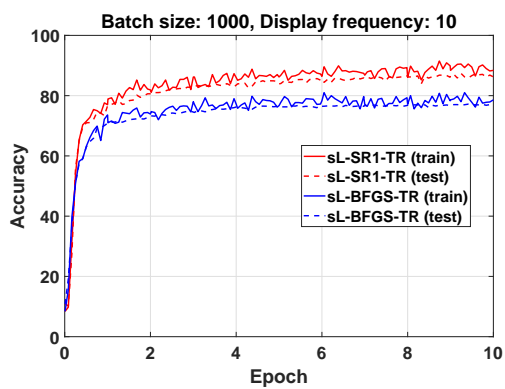
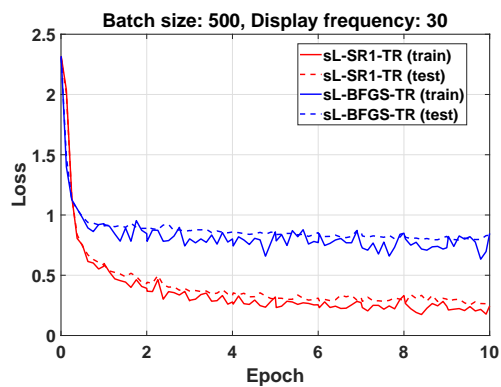
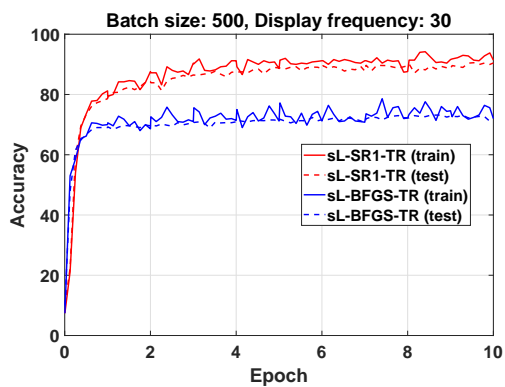
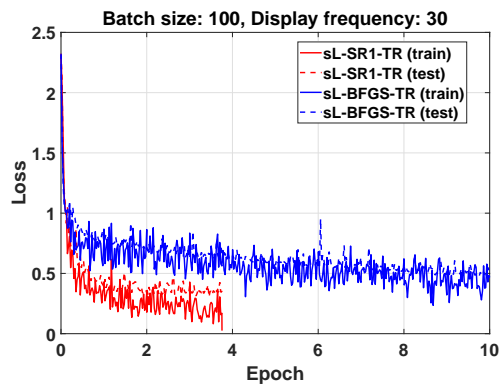
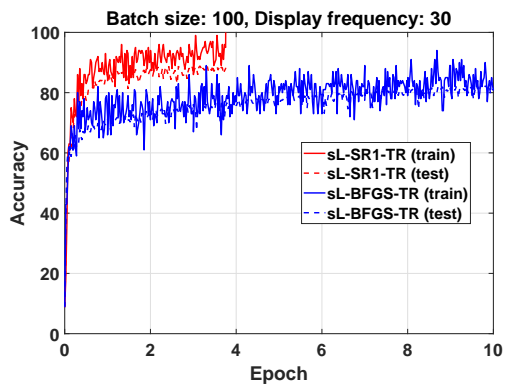
^a $\epsilon = 10^{-5}$, $\text{epoch}_{max} = 10$, $\gamma_0 = 1$, $\delta_0 = 1$, $\tau_1 = 10^{-4}$, $\tau = 10^{-8}$

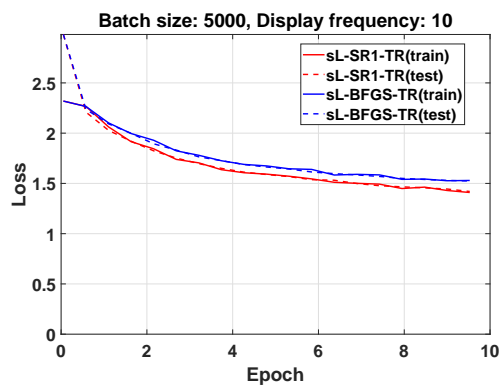
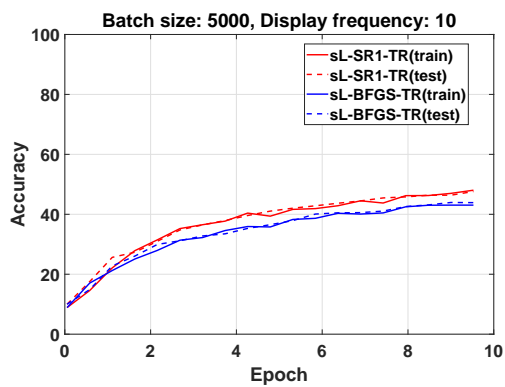
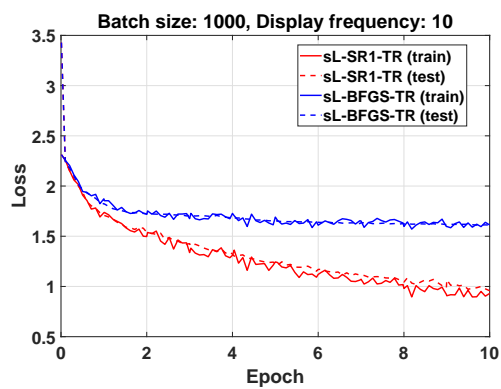
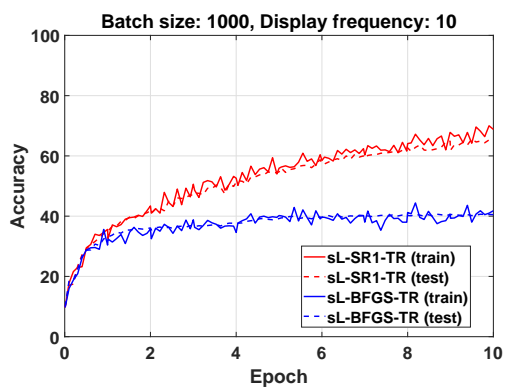
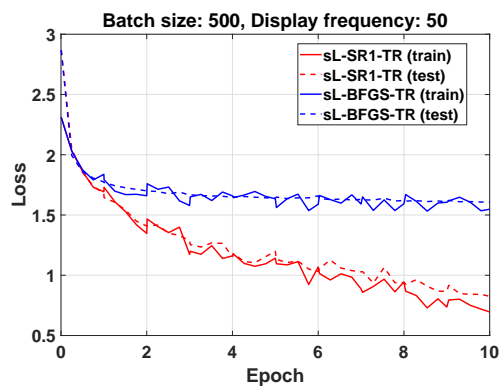
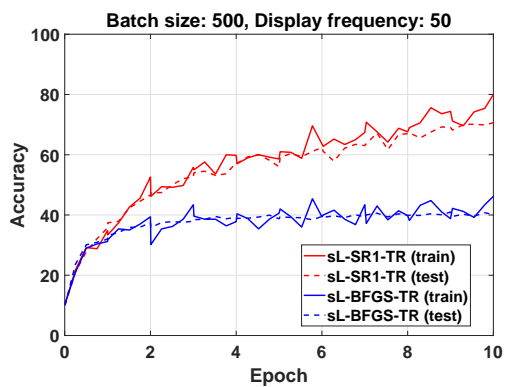
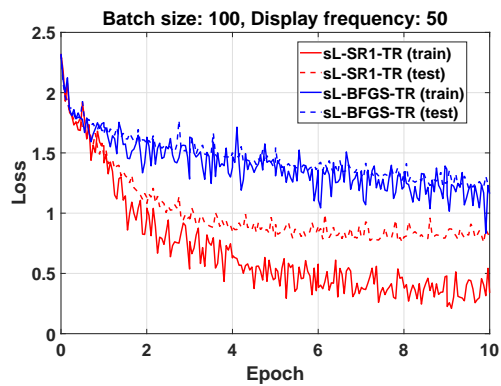
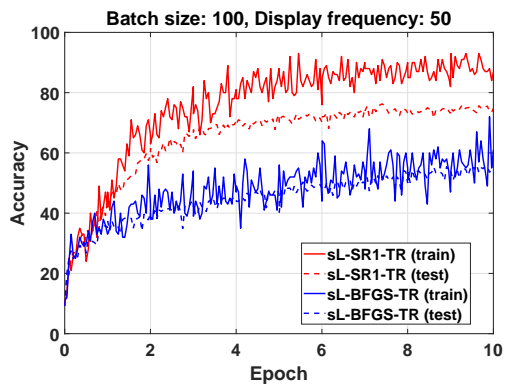


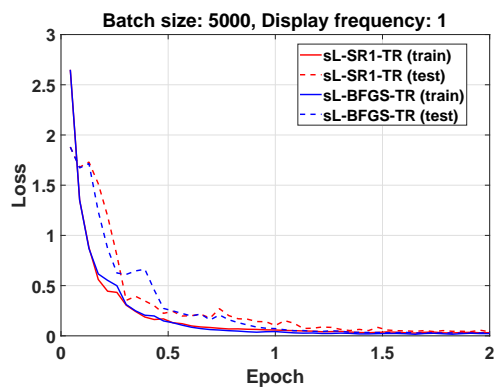
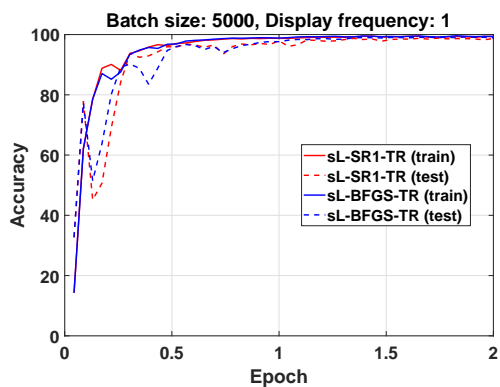
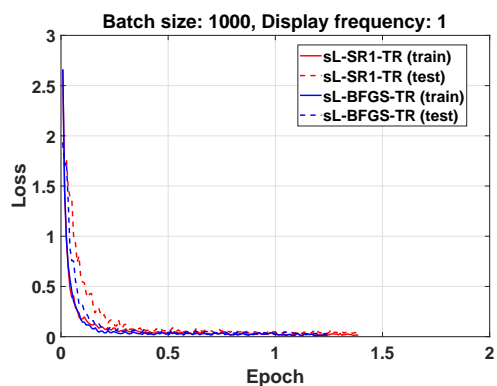
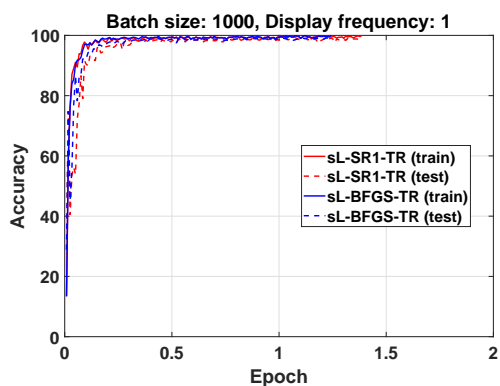
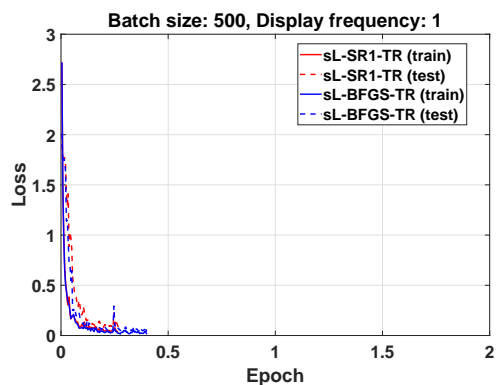
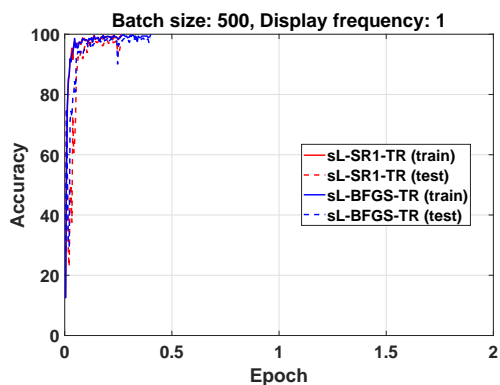
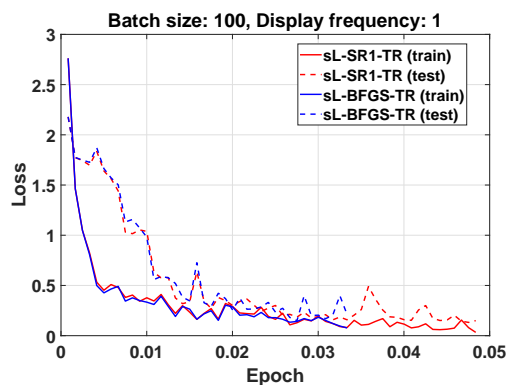
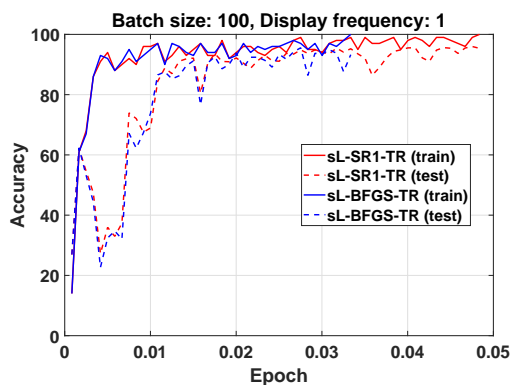


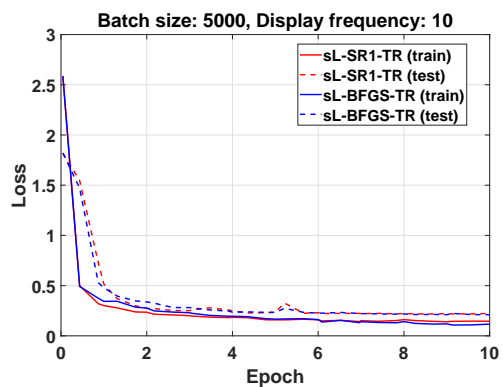
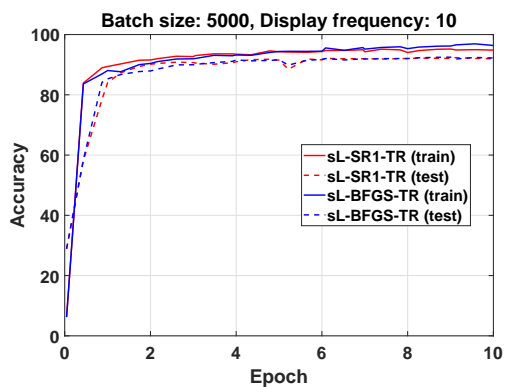
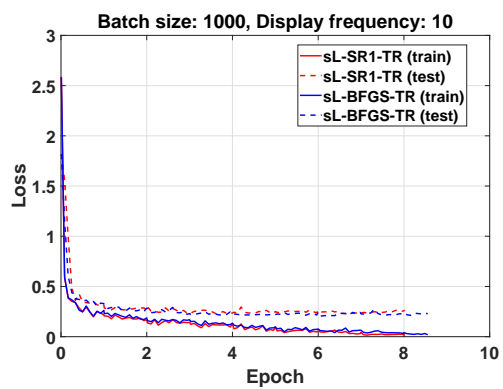
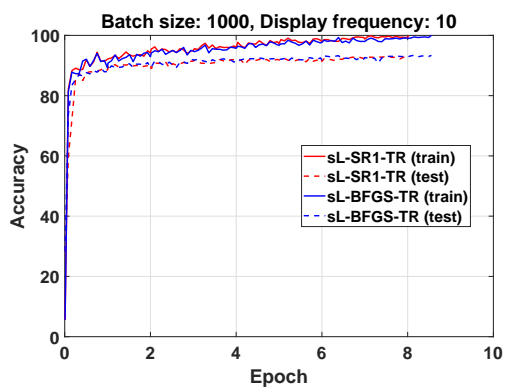
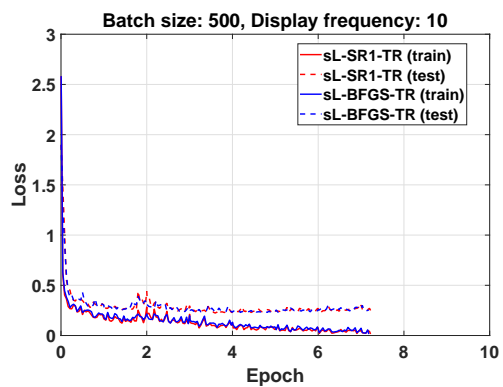
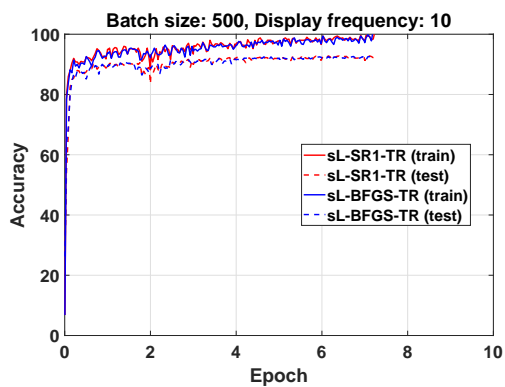
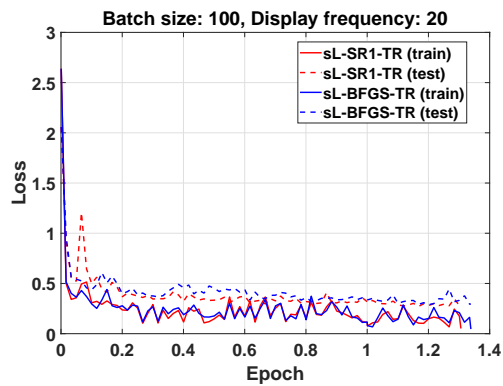
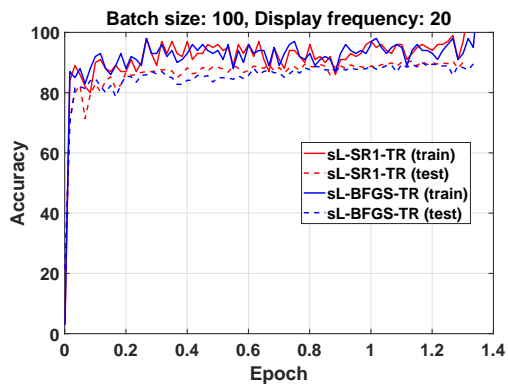


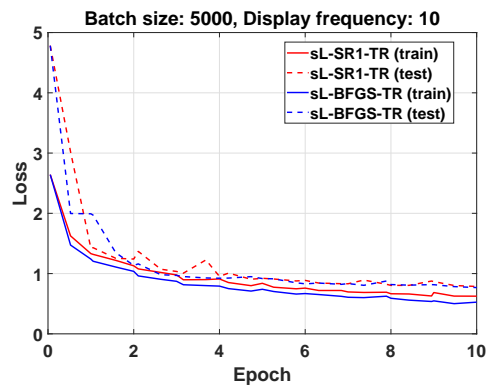
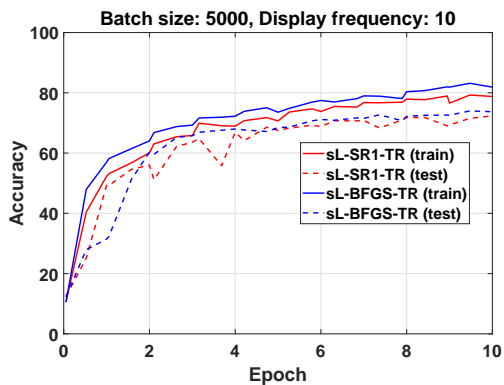
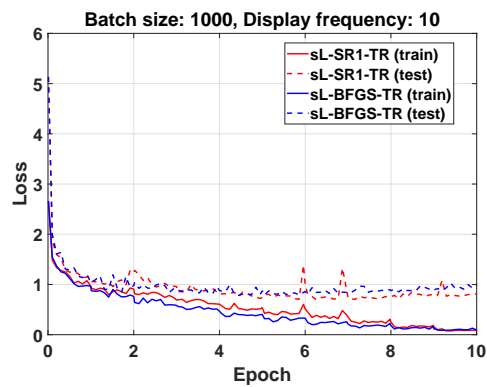
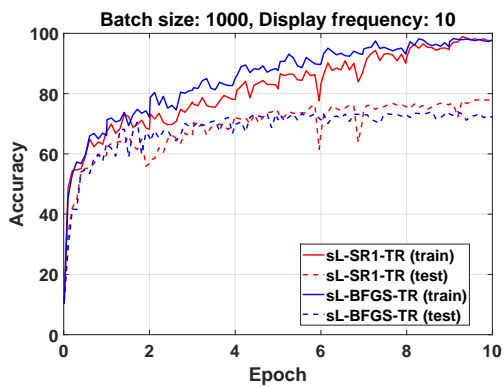
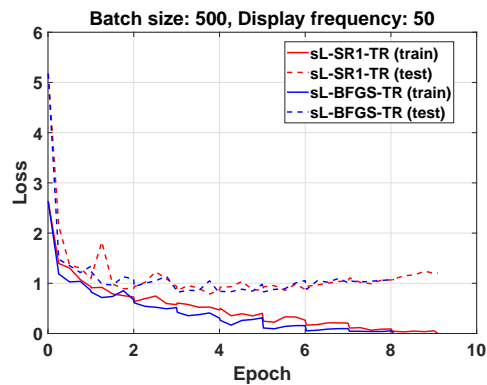
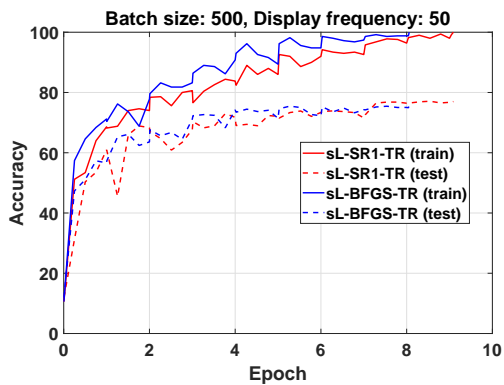
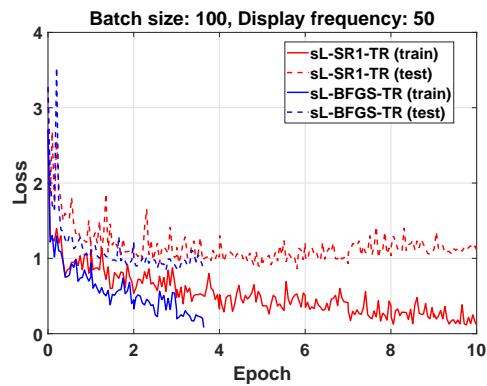
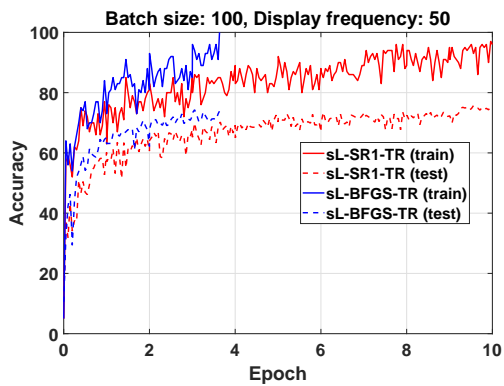


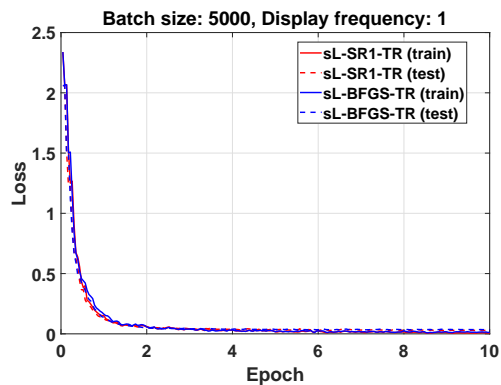
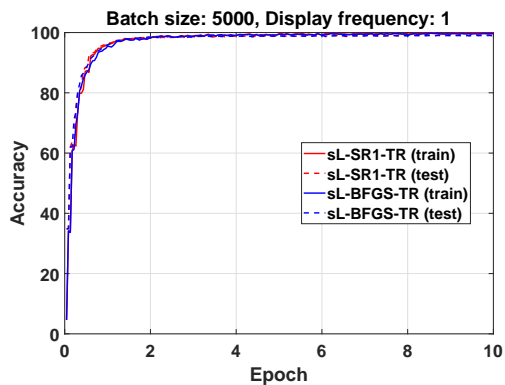
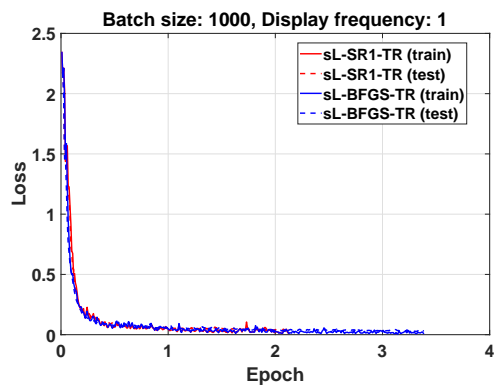
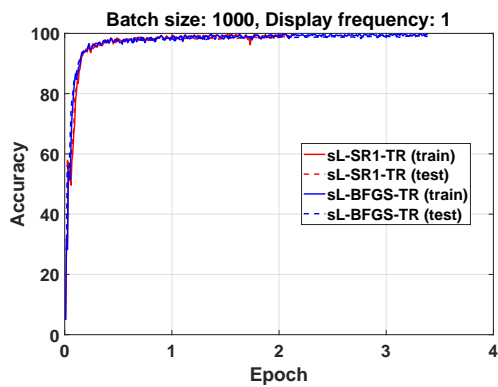
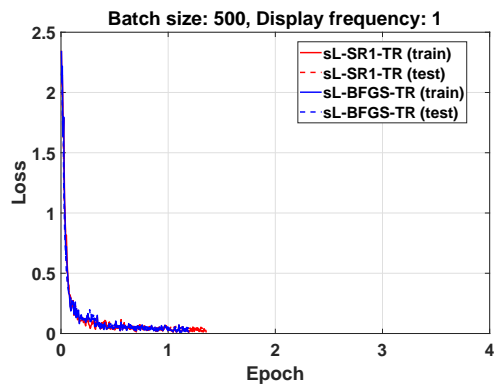
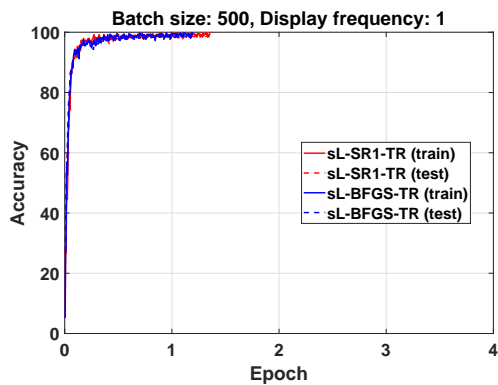
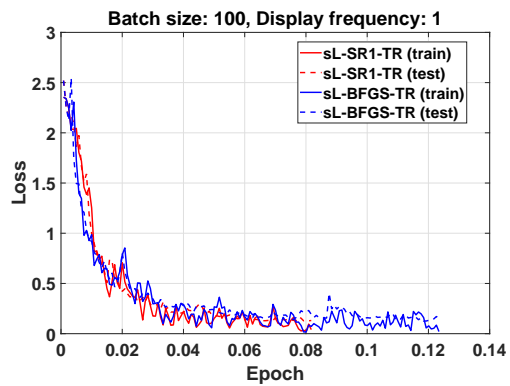
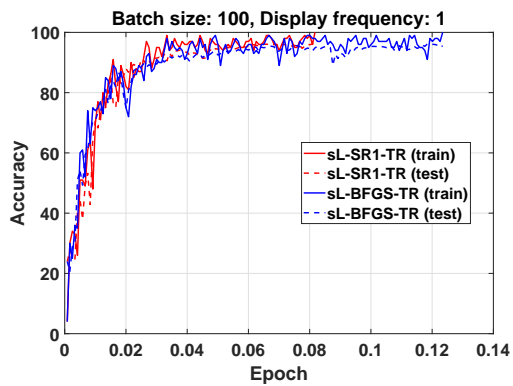


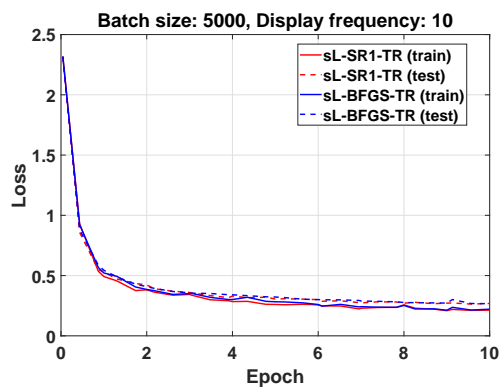
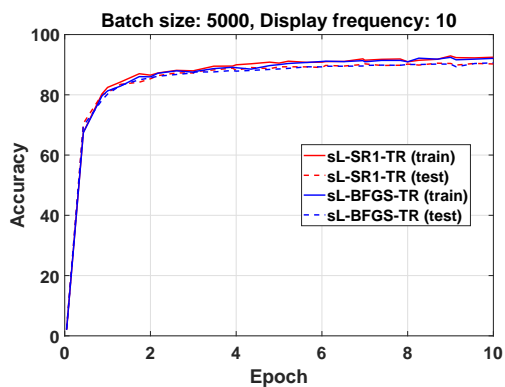
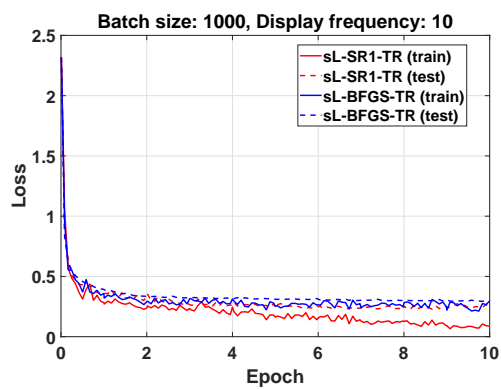
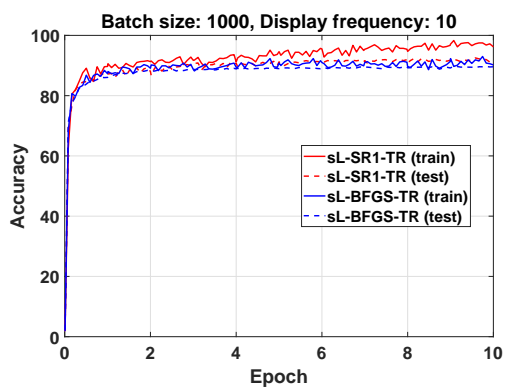
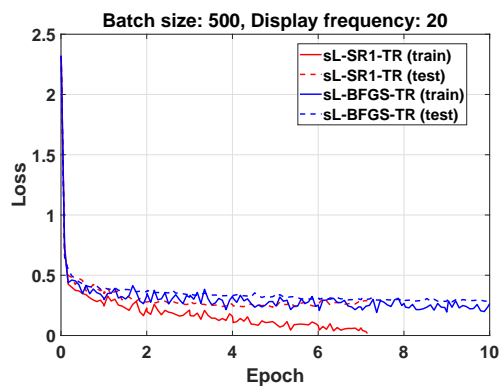
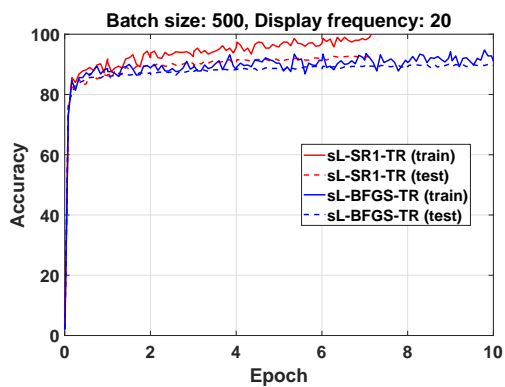
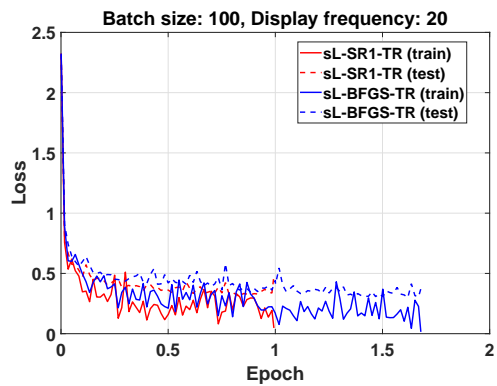
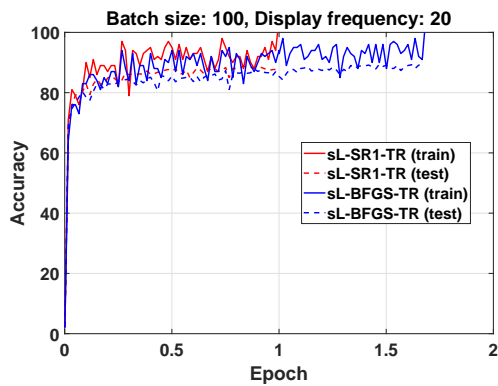


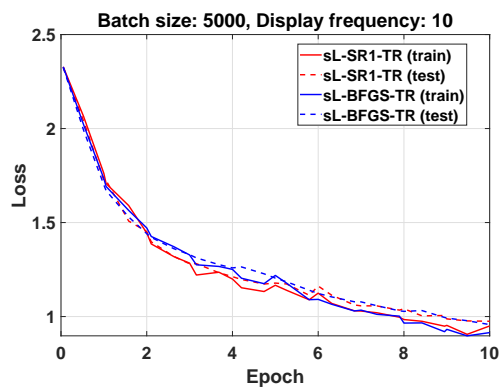
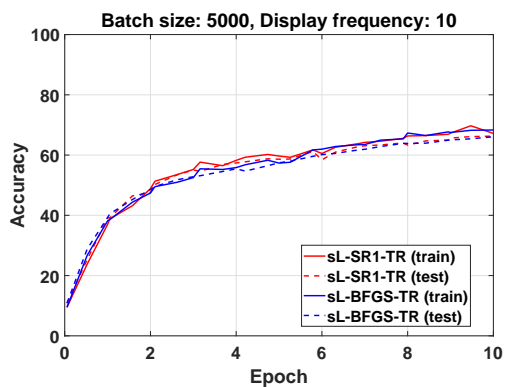
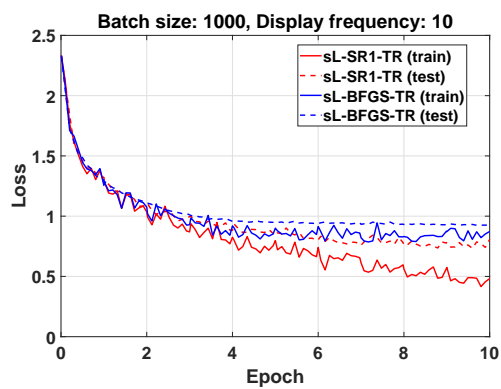
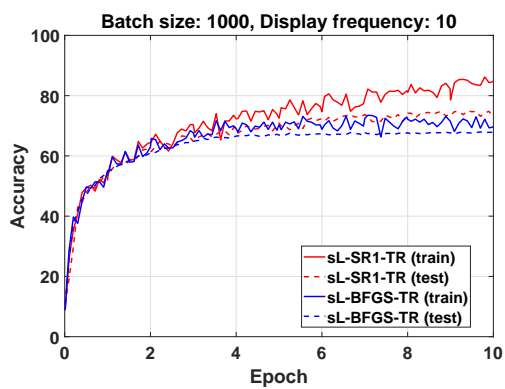
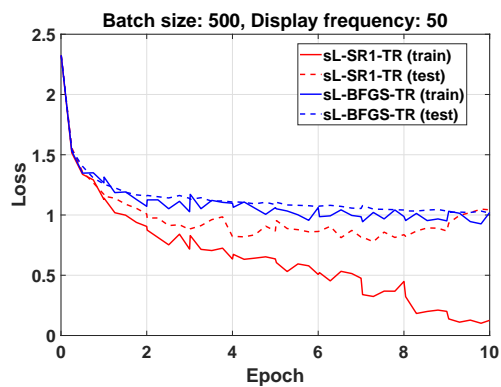
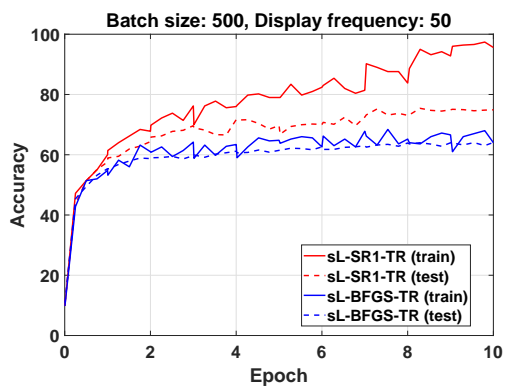
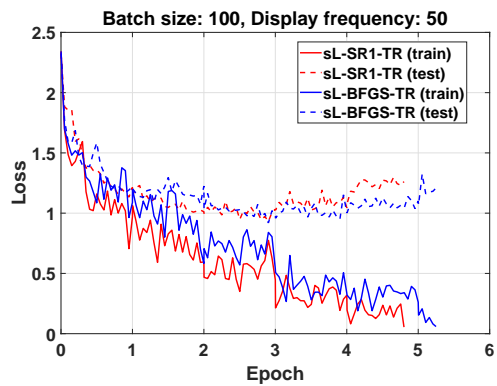
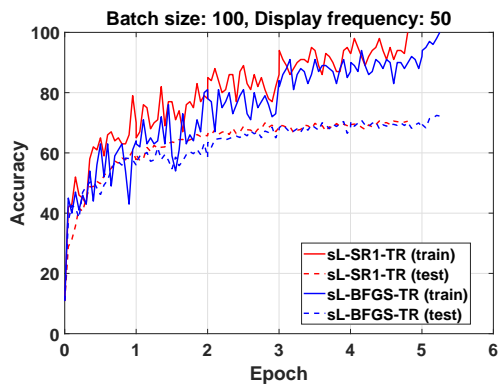


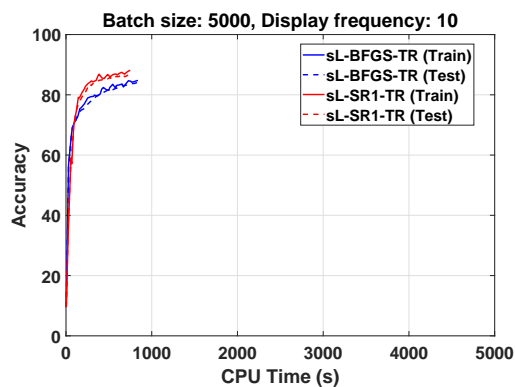
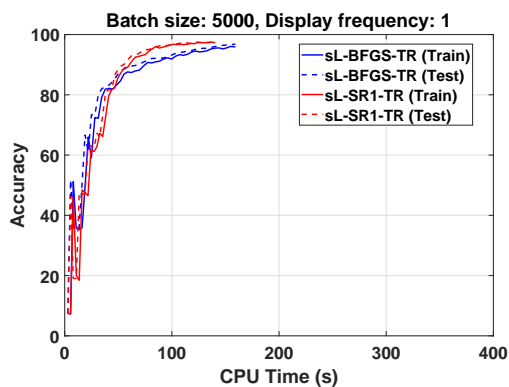
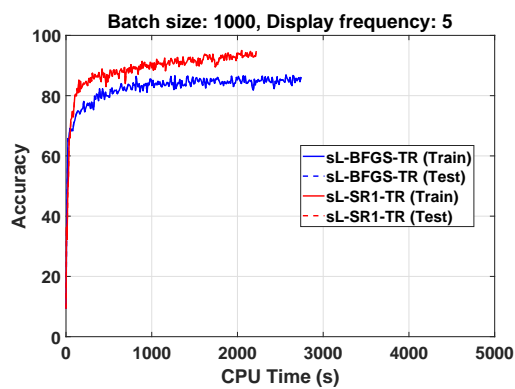
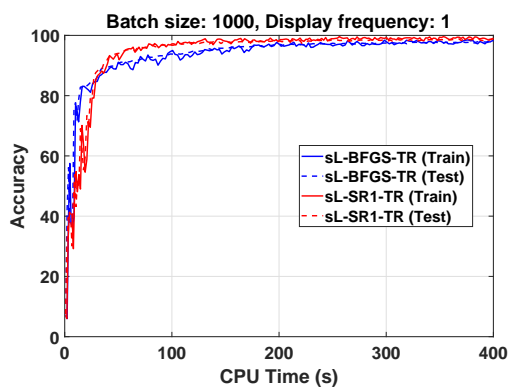
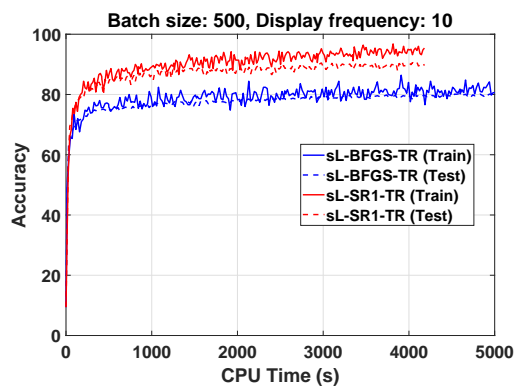
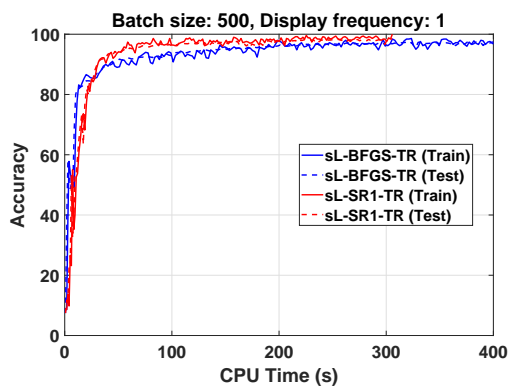
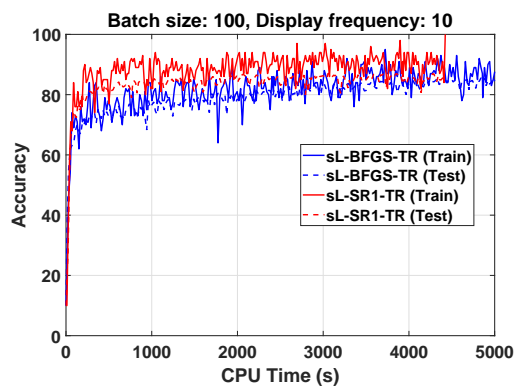
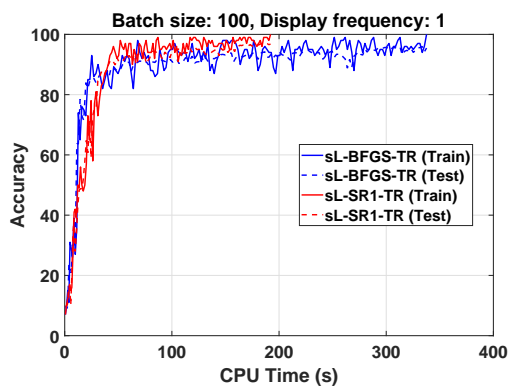






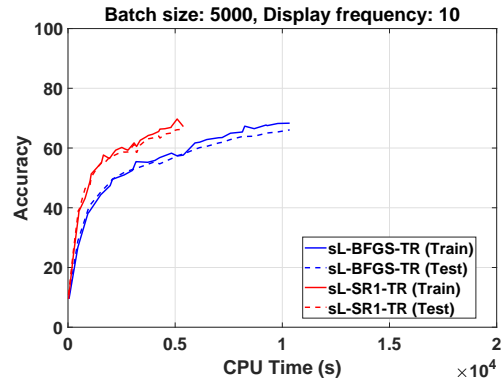
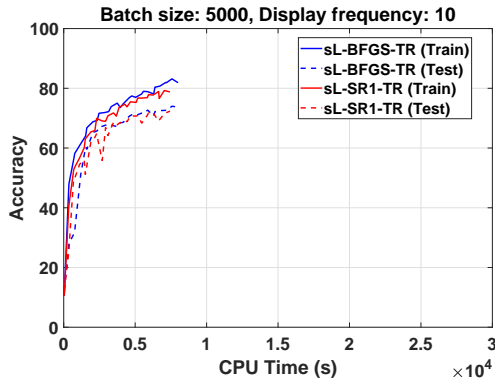
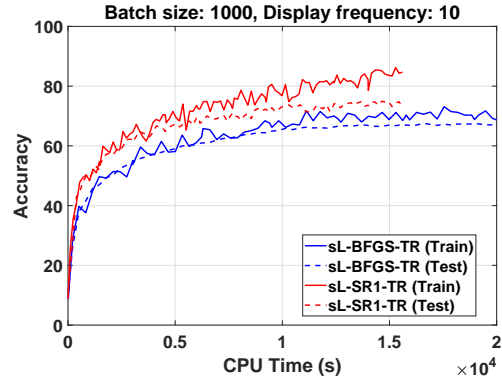
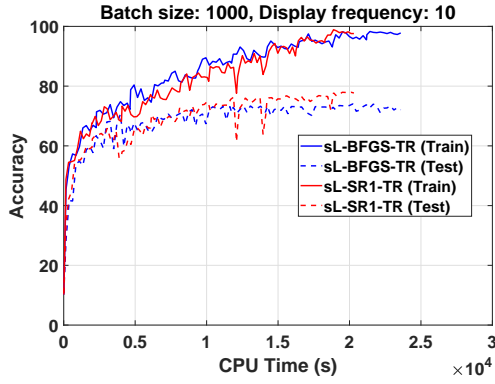
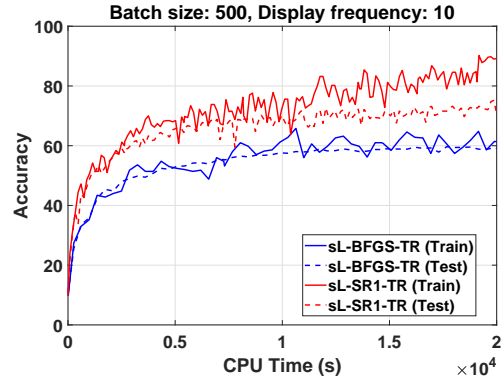
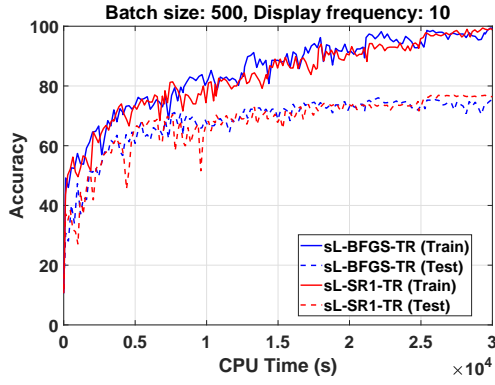
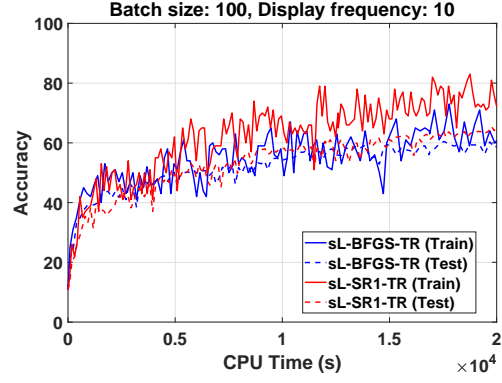
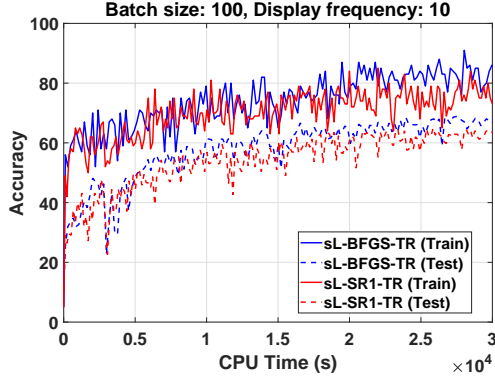






(a) MNIST, LeNet-like

(b) Fashion-MNIST, LeNet-like



(a) CIFAR10, ConvNet3FC2

(b) CIFAR10, ConvNet3FC2(no BN)

